Clim. Past, 21, 919–939, 2025
https://doi.org/10.5194/cp-21-919-2025

Climate of the Past
Open Access
EGU

The Early–Middle Pleistocene Transition in the Gulf of Cadiz (NE Atlantic) – an interplay between subtropical gyre and extremely cold surface waters

Aline Mega[1,2], **Teresa Rodrigues**[1,2], **Emília Salgueiro**[1,2], **Mária Padilha**[1], **Henning Kuhnert**[3], and **Antje H. L. Voelker**[1,2]

[1]Divisão de Geologia e Georecursos Marinhos, Instituto Português do Mar e da Atmosfera (IPMA), Avenida Doutor Alfredo Magalhães Ramalho 6, 1495-165 Alges, Portugal
[2]Centro de Ciências do Mar (CCMAR/CIMAR LA), University of the Algarve, Campus de Gambelas, 8005-139 Faro, Portugal
[3]MARUM, Universität Bremen, Leobener Straße 8, 28359 Bremen, Germany

Invited contribution by Aline Mega, recipient of the EGU Climate: Past, Present & Future Outstanding Student Poster and PICO Award 2019.

Correspondence: Aline Mega (alinemega20@gmail.com)

Received: 14 October 2024 – Discussion started: 25 October 2024
Revised: 11 February 2025 – Accepted: 21 February 2025 – Published: 20 May 2025

Abstract. Besides the shift in dominant orbital cyclicity depicted in paleoclimate proxy records, the Mid-Pleistocene Transition or Early–Middle Pleistocene Transition (EMPT) was linked to a change in the deep thermohaline circulation. Those changes contributed to more intense and longer-lasting glacial periods and cooler sea surface temperatures (SSTs) during glacials. Within the Atlantic Ocean, the Iberian Margin is considered a key location to study climatic variations influenced by both high- and low-latitude processes. In this study we focus on IODP Site U1387 on the southern Portuguese margin to reconstruct surface water circulation changes and related plankton foraminifera ecosystems during the interval of Marine Isotope Stage (MIS) 28 to MIS 18 (1006–750 ka). Our planktonic foraminifera assemblages and SST reconstructions (foraminifera assemblages and $U^{K'}_{37}$ alkenone index) demonstrate warm, relative stable SST conditions during much of the interval due to persistent influence of subtropical gyre waters as indicated by the tropical–subtropical and Azores Current-related foraminifera species and the periods with dominant sinistral coiling direction of the species *Globorotalia truncatulinoides*. Maximum interglacial SSTs were up to 2 °C warmer than at present in both summer and winter, with the exception of interglacial MIS 23 with SSTs ∼ 1.5 °C colder than in the other interglacials. Subsequent to the respective glacial inception, the relatively warm conditions were periodically interrupted by millennial-scale extreme cold events when polar species *Neogloboquadrina pachyderma* became abundant (> 30 %), and the SSTs, reconstructed from the foraminifera assemblage data, dropped below 10 °C in summer and 5 °C in winter, although some of those values might be overestimated. The most pronounced event, considering the amplitude of cooling and duration, occurred between 870 and 864 ka, marking the terminal stadial event of the MIS 22–MIS 21 transition (Termination X). Extreme cold events, always associated with the incursion of subpolar waters into the Gulf of Cadiz, mark all the terminal stadial events from Terminations XII to IX and the millennial-scale variability during the transitions to full glacial conditions, although the duration of the cooling varied greatly. The extreme cooling was only possible through migration of the subarctic front into the lower mid-latitudes as a consequence of cooling and freshening in the higher latitudes and the associated extreme reduction in the Atlantic Meridional Overturning Circulation. The amplitude of cooling, duration, and frequency of subpolar water incursions during MIS 24 to MIS 22 stands out, providing further evidence for the "900 ka event" being a key feature of the EMPT.

1 Introduction

A major global climatic shift, known as the Mid-Pleistocene Transition or Early–Middle Pleistocene Transition (EMPT), took place between 1250 and 650 ka, dramatically changing Earth's climate dynamics (Clark, 2012; Clark et al., 2006; Head and Gibbard, 2015; McClymont et al., 2013). This period was characterized by long-term cooling in global mean sea surface temperatures (SSTs); lower glacial atmospheric carbon dioxide levels; and a change in the deep-water circulation, stratification, and carbon storage during the glacial periods, which led to more intense and longer-lasting glacial periods (changing from 41 to 100 kyr cycles) and cooler SSTs (Chalk et al., 2017; Clark et al., 2024; Farmer et al., 2019; Kim et al., 2021; Tachikawa et al., 2021; Willeit et al., 2019; McClymont et al., 2013). Early studies (Farmer et al., 2019; McClymont et al., 2013; Pena and Goldstein, 2014) described a major shift in the deep-water circulation during the EMPT, often considered as the first 100 kyr cycle and referred to as the "900 ka event". The new high-resolution time series of Hines et al. (2024) revealed, however, no substantial changes in deep-ocean circulation across the EMPT, and the authors attributed the observed shift in deep-ocean carbon storage to changes in deep-ocean density stratification, with Southern Ocean conditions playing an important role.

The causes of the long-term patterns of Quaternary climate have been attributed to internal changes in climate response to orbital forcing, as the latter did not change over this time (Clark, 2012; Clark et al., 2006; Hodell and Channell, 2016; Shacketon, 2000). It is believed that the EMPT may have been influenced by ocean–atmosphere system changes, with declining atmospheric carbon dioxide concentrations and continental ice-sheet growth playing a role (Chalk et al., 2017; Willeit et al., 2019). During the EMPT glacials, lower sea levels contribute to benthic δ^{13}C values reaching their lowest levels in 5 million years (Westerhold et al., 2020), which may be caused by exposed continental shelves accelerating the transport of organic carbon into the oceans (Head and Gibbard, 2015). Nowadays, water masses carrying lower δ^{13}C signals (< 0.5 ‰) are formed by convection around Antarctica (Antarctic Intermediate Water, Antarctic Bottom Water (AABW)) and spread out into the global ocean basins (Curry and Oppo, 2005; Kroopnick, 1985). Northward and upward expansion of such signals in the Atlantic basin during glacial periods was therefore interpreted to reflect the replacement of North Atlantic Deep Water (NADW) by southern sourced waters and thus a reduced Atlantic Meridional Overturning Circulation (AMOC) (Hodell and Channell, 2016; Raymo et al., 2004, 1990; Sarnthein et al., 1994). A recent data–model comparison for the Last Glacial Maximum suggests, however, that benthic δ^{13}C signals in the deep ocean and associated shifts in prevailing water masses should be interpreted as reflecting AMOC depth and not AMOC strength (Muglia and Schmittner, 2021). Throughout the MIS 22–MIS 24 interval, weakening NADW influence is further indicated by neodymium isotope records (Farmer et al., 2019; Kim et al., 2021; Pena and Goldstein, 2014; Tachikawa et al., 2021), although the new record from IODP Site U1479 in the South Atlantic revealed substantial NADW presence during MIS 23 (Hines et al., 2024). A possible explanation for the increase in glacial δ^{18}O values during the 900 ka event relates a weak AMOC and low insolation in the Southern Hemisphere during Marine Isotope Stage (MIS) 23 to maximum continental ice volume build-up, which continued to be recorded in the subsequent glacials (Elderfield et al., 2012; Pena and Goldstein, 2014). Hines et al. (2024), on the other hand, attribute the signal to increased density stratification between northern-sourced (NADW) and southern-sourced waters (AABW) and the shoaling of the boundary between those water masses.

Most of the water stored during Quaternary glaciations in the Laurentide, Greenland, and European ice sheets was discharged into the North Atlantic Ocean during the last 1.5 Myr, producing short, cold events that were often associated with ice-rafted debris (IRD) deposition (Barker et al., 2022, 2021; Hodell and Channell, 2016; Jansen et al., 2000). The effect of ice-cover changes during the EMPT, mainly associated with the 900 ka event, has been reported based on different proxies and in the (sub)polar regions of both hemispheres. In the North Atlantic, Wright and Flower (2002) found extremely cold events from 1000 to 500 ka at ODP Sites 980 (55° N, 15° W) and 984 (61° N, 24° W) (Fig. 1), based on the percentage of polar species *Neogloboquadrina pachyderma* and IRD records, later on corroborated by the 1.7 Myr long records for Site 983 (60° N 24° W) (Barker et al., 2011, 2022). These data, in conjunction with increased reworked nannofossil abundance during the IRD events at Sites 980/981 (Marino et al., 2011), suggest that the Arctic front shifted from a position between those sites southward, and the sea-ice cover expanded greatly during those periods. That scenario is supported by evidence from IODP Site U1314 (56.36° N, 27.88° W), where Hernández-Almeida et al. (2013) observed an abundance of *N. pachyderma* of up to 93 % during the 900 ka event. Between 900 and 675 ka, the same, short-term extreme cold events were registered further south at IODP Site U1385 (Iberian Margin) as cold SST events associated with lower salinities (higher percentages of the C37:4 alkenone) (Rodrigues et al., 2017). All those cold events were associated with a northward and upward penetration of AABW into the mid-latitudinal North Atlantic (Hodell and Channell, 2016; Hodell et al., 2023a; Hernández-Almeida et al., 2015), implying a reduction in the AMOC depth (Muglia and Schmittner, 2021), especially during the terminal stadial events.

The western Iberian Margin is a key area for high-resolution paleoclimatic studies because it is climatologically sensitive to high- and low-latitude processes. Following the seminal work of Shackleton et al. (2000), it is known that benthic foraminifera δ^{18}O records from depths greater than 2500 m on the southwestern Portuguese mar-

gin reflect an Antarctic climate signal, in particular Antarctic temperature variations, whereas surface water records from the western and southern Portuguese margin mimic the millennial-scale Greenland interstadial–stadial oscillation and thus record Northern Hemisphere temperature variations. This concept has now been demonstrated for the last 1440 kyr with the high-resolution records of IODP Site U1385 (Hodell et al., 2015, 2023a).

Furthermore, planktonic foraminifera assemblages are reliable sources for environmental conditions in the western Iberian Margin and specific assemblages can identify prevailing oceanographic conditions. In modern conditions, subtropical species, among them *Globigerinoides ruber* (white), reflect the influence of the Azores Current (AzC), whereas *Globigerina inflata* and *Neogloboquadrina incompta* represent the Portugal Current and *Globigerinoides bulloides* upwelling events (Salgueiro et al., 2008). Increased abundances of *Turborotalita quinqueloba* and *Neogloboquadrina pachyderma*, on the other hand, can provide insights into past incursions of subpolar waters and southward displacement of the subarctic front (boundary between the subtropical and subpolar gyres) (Eynaud et al., 2009; Girone et al., 2023; Johannessen et al., 1994; Martin-Garcia et al., 2015; Pflaumann et al., 2003; Salgueiro et al., 2010; Singh et al., 2023).

Recent studies (Bajo et al., 2020a; Voelker et al., 2015a) confirmed extremely cold SST conditions during stadial climate events of the EMPT also at southern Portuguese margin IODP Site U1387 (Fig. 1). However, detailed information on the surface-water conditions during the 900 ka event (MIS 24 to MIS 22) and during the lead up to it remains limited. This study, therefore, aims to characterize surface-water conditions at IODP Site U1387 between MIS 28 and MIS 18 (1006–750 ka) to better understand the climate dynamics and oceanographic changes that occurred during this critical period. Situated in the northern Gulf of Cadiz, Site U1387 is highly sensitive to changes in the North Atlantic subtropical gyre and to the water mass exchange between the North Atlantic and the Mediterranean Sea. Moreover, the high sedimentation rates ($\geq 20\,\mathrm{cm\,kyr^{-1}}$) in contourite drifts like the Faro drift, into which Site U1387 was drilled, provide exceptional paleoclimate records with high temporal resolution (Hernández-Molina et al., 2016b). For evaluating temperature changes, in terms of both amplitude and timing, and their relationship to the prevailing oceanographic conditions, we produced high-resolution, sub-millennial-scale records of planktonic foraminifera assemblages and SST reconstructions. Using a multi-proxy approach, the SSTs were reconstructed in two ways: (1) converting the planktonic foraminifera assemblages into summer and winter SSTs using a transfer function and (2) based on the $U^{K'}_{37}$ alkenone index, approximately reflecting annual mean SSTs. Conditions in the subtropical gyre were also inferred from the dominant coiling direction of the planktonic foraminifera species *Globorotalia truncatulinoides* (% GTS) (Billups et al., 2016), although apparent inconsistencies between that proxy data (Billups et al., 2016, 2020) and the gyre strength reconstruction of Wharton et al. (2024) for the Last Glacial Maximum still need to be solved. We compare our data with other available records from the southwestern Iberian Margin, as well as sites from the mid-latitudinal North Atlantic. This comparison allows us to contextualize our results within broader regional and global climatic trends, providing insights into the variability and connections between these key areas during the study period. By integrating these records, we aim to improve our understanding of both local and large-scale processes affecting this northeast Atlantic region.

2 Regional setting

The subtropical gyre nowadays comprises much of the surface and sub-surface waters in the low- to mid-latitudinal North Atlantic, is approximately 1000 km in diameter, and distributes heat and moisture to the north (Fig. 1a). The gyre circulation is driven by a combination of trade winds, westerlies, and the Coriolis force, whereby the westerlies dominate the circulation in its northern part, especially during the winter. The strength and position of the oceanic currents depend, therefore, on the variability of the atmospheric wind fields. During the winter the latter are characterized by the eastward displacement of cyclonic perturbations (Relvas et al., 2007).

Located within the southern mid-latitudinal North Atlantic, the Gulf of Cadiz has a surface–subsurface current system dominated by three branches of the North Atlantic's subtropical gyre circulation: the eastward-flowing AzC between 34.3 and 35.7° N, contributing with heat and salt; the Azores Countercurrent between 37.74 and 39.24° N; and the Canary Current that flows southwestwards (Carracedo Segade et al., 2015). The AzC dominates the Gulf of Cadiz surface waters (0 to 500 m) and partially recirculates along the western Iberian Margin through the Iberian Poleward Current that results from the seasonal reversal of the wind regimes (Frouin et al., 1990; Peliz et al., 2005) (Fig. 1b). Also, the Gulf of Cadiz is an important transition zone where the Mediterranean Outflow Water flows at an intermediate depth level, adding high salinity and heat to the North Atlantic Circulation (Ambar et al., 1999; Folkard et al., 1997).

The Gulf of Cadiz receives contributions from the Portugal Current and the Portugal Coastal Current (Fiuza et al., 1998). The Portugal Current flows equatorward transporting cooler and less saline waters into the region (Carracedo et al., 2014; Peliz et al., 2009). The Portugal Coastal Current only exists during the upwelling season from late May–early June to late September–early October, driven by the northerly winds that transport cold and less saline upwelled water (jet-like) southward (Criado-Aldeanueva et al., 2006; Folkard et al., 1997) (Fig. 1b). Near Cape St. Vincent, a part of the Portugal Coastal Current jets turns eastward under favorable wind conditions and enters the Gulf of Cadiz, flowing along the upper slope toward the Strait of Gibraltar, interacting with

the upwelling off Cape Santa Maria (Sanchez and Relvas, 2003) and affecting the region of Site U1387.

The Gulf of Cadiz SSTs have a seasonal behavior observed by Folkard et al. (1997) through satellite images. Temperatures vary between 22.5 °C (summer) (Fig. 1b) and 16.5 °C (winter), with a mean value of 19.6 °C (Vargas et al., 2003).

3 Material and methods

IODP Site U1387 (36°48.3210′ N, 7°43.1321′ W) was drilled in December 2011 by the Integrated Ocean Drilling Program (IODP) during Expedition 339 – Mediterranean Outflow into the Faro Drift, northern Gulf of Cadiz, at a water depth of 559 m (Fig. 1) (Expedition 339 Scientists, 2013). The samples were collected at a resolution of 12–13 cm along the revised splice (Voelker et al., 2018), except for the interval of Termination X, where the resolution was increased to 6–7 cm for the Bajo et al. (2020a) study. Each sample was freeze-dried, weighed, and washed through a 63 µm mesh sieve, following the procedure established in the Sedimentology and Micropaleontology Laboratory of the Division for Geology and Marine Georesources at the Portuguese Institute for the Sea and Atmosphere (IPMA) (Voelker et al., 2015a). The coarse-fraction residue was transferred onto filter paper, dried at 40 °C, and weighed.

3.1 Stable isotope measurements

To establish a stable oxygen isotope record for the chronostratigraphy, 6–12 specimens of the planktonic foraminifera *Globigerinoides bulloides* were collected from the fraction > 250 µm of a total of 706 samples. The specimens were sent to the gas isotope ratio mass spectrometry laboratory at MARUM (University Bremen), Germany, where they were analyzed with a Finnigan MAT-251 or MAT-252 mass spectrometer coupled to an automated Kiel I or Kiel III carbonate preparation system, respectively. The mass spectrometers' long-term precision is ± 0.07 ‰ for δ^{18}O based on repeated analyses of internal (Solnhofen limestone) and external (NBS-19) carbonate standards. Some of the isotope results were already published in Bajo et al. (2020a) and are available in Bajo et al. (2020b), although the age model used in the current study differs from those data.

3.2 Planktonic foraminifera assemblage analysis and SST calculations

For the planktonic foraminifera assemblage, a total of 356 samples were analyzed at a sample resolution of 24–25 cm. Each sample was dry-sieved to obtain the fractions > 250 µm and 150–250 µm. The respective fraction was then split until about 200 specimens remained in the fraction > 250 µm and about 100 specimens in the 150–250 µm fraction. Specimens, including identifiable fragments, were counted and identified in full in each sub-split.

Species identification followed Kučera (2007) and Schiebel and Hemleben (2017). All sinistral coiling *Neogloboquadrina pachyderma* specimens were assigned to *N. pachyderma*, in agreement with the observed morphotypes being similar to those typically found in polar regions (Fig. S1 in the Supplement). We are using the percentage of *N. pachyderma* to identify cold-water incursions of subpolar origin into the Gulf of Cadiz. The assemblage data were converted into relative abundances (percentages) and species grouping into tropical/subtropical, transitional, and subpolar/polar habitats according to Kučera (2007). The Azores Current factor was calculated following Salgueiro et al. (2008) and combines the percentages of *Globorotalia inflata*, *Globigerinoides ruber* (white), and *Trilobatus sacculifer*.

To evaluate changes related to the subtropical gyre influence, we used the newly developed proxy of the coiling direction of planktonic foraminifera *G. truncatulinoides*, which is a subsurface dwelling species with five morphotypes. The morphotype type II is exclusive of the Atlantic Ocean and the Mediterranean Sea and is the only type with dextral and sinistral forms (de Vargas et al., 2001; Ujiié et al., 2010). According to Billups et al. (2016), the amount of sinistral coiling direction of this species increases when the subtropical gyre circulation is more intense. Kaiser et al. (2019) related it furthermore to water temperatures at 300 m (≥ 12 °C) and thus the vertical expansion of the warm water sphere of the subtropical gyre. The proxy will be applied for the first time at the eastern margin of the North Atlantic subtropical gyre. Based on the % GTS distribution along the gyre's eastern margin (Fig. S2; see also Fig. 1 in Kaiser et al., 2019) and the western and southern Iberian margin in particular, where higher % GTS values are observed in the regions under AzC and thus warmer, subtropical waters influence (Fig. 1), we are confident that the proxy can be used in our region. For obtaining the % GTS data, whenever possible, we analyzed all the individuals in the fraction > 250 µm in all the samples where this species was found (332 of 356 samples screened). Intervals with a high sample volume were split before size fractioning. The coiling ratio was obtained using the following formula: $\%\ \mathrm{GTS} = \mathrm{GTS} \cdot 100 \cdot (\mathrm{GTS} + \mathrm{GTD})^{-1}$, where GTS is the number of sinistral specimens and GTD the number of dextral specimens (Billups et al., 2016; Ducassou et al., 2018). Kaiser et al. (2019) established that % GTS values for the interpretation of paleoceanographic conditions should be based on the counts of ≥ 20 specimens.

Using the relative abundance data in the assemblages, we estimated the SST for winter and summer using the non-distance-weighted (ndw) option of the SIMMAX program (Pflaumann et al., 1996), similar to the Modern Analog Technique (MAT), following Salgueiro et al. (2014). Although Jonkers and Kučera (2019) recently showed that only 10 species dominate the SST calculations, we used the complete set of 27 species utilized by Pflaumann et al. (1996)

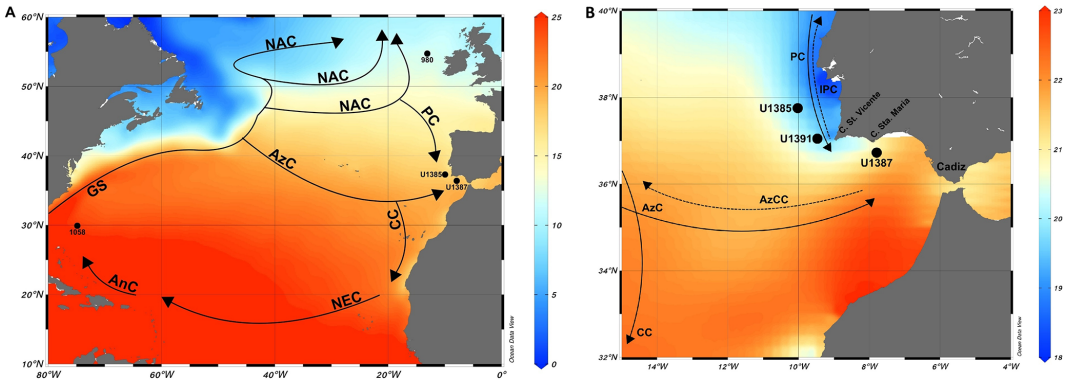

Figure 1. **(a)** North Atlantic Ocean with annual mean SSTs (°C) at 0.25° resolution as background (WOA 2023; Reagan et al., 2024). Location of IODP Site U1387 and other available North Atlantic records discussed in the text (IODP Site U1385, ODP Site 980, ODP Site 1058, DSDP Site 607/IODP Site U1313). Black arrows represent the surface circulation: GS – Gulf Stream, NAC – North Atlantic Current, PC – Portugal Current, CC – Canary Current, AzC – Azores Current, NEC – North Equatorial Current, AnC – Antilles Current. **(b)** Close-up of the study area with locations of IODP Site U1387 and SW Iberian Margin IODP Sites U1385 and U1391, with the mean summer (July–September) SSTs (°C) at 0.25° resolution as the background (WOA 2023; Reagan et al., 2024). Black arrows represent the surface circulation: AzCC – Azores Countercurrent, IPC – Iberian Poleward Current. Currents adapted from Baptista et al. (2021) and references therein. Background maps made with ODV (Schlitzer, 2023).

to be consistent with previous reconstructions in the region (Salgueiro et al., 2014, 2010). SST was calculated using 10 nearest neighbors and the modern analog database compiled by Salgueiro et al. (2014), which combines the North Atlantic database of the MARGO project (Kučera et al., 2005) with additional samples for the Iberian Margin (Salgueiro et al., 2008) and off NW Africa (Salgueiro et al., 2014; Voelker and Salgueiro, 2017).

3.3 Alkenone SST reconstructions

We also reconstructed SSTs based on the alkenone $U^{K'}_{37}$ index. Alkenones are lipid molecules that are synthesized by coccolithophorid (phytoplankton) and can be extracted from marine sediments using organic solvents. Lipid molecule analyses were done at 24–25 cm resolution (same levels as planktonic foraminifera assemblage data), except for Termination X, where the resolution increased to 6–7 cm (Bajo et al., 2020c). Lipid biomarker extraction was done in 338 samples, whereby the SST for the 216 samples between 212.3 and 257.9 cmcd were already published in Bajo et al. (2020a). Extraction of lipid molecules from freeze-dried sediments followed the procedure established in the DivGM's Biogeochemistry Laboratory (Rodrigues et al., 2017; Voelker et al., 2015a), which is based on Villanueva et al. (1997). The di-, tri-, and tetra-unsaturated alkenones of 37 carbon atoms were analyzed in a Varian gas chromatograph model 3800 equipped with a septum programmable injector and a flame ionization detector (GC-FID) with a CPSIL-5 CB column. Hydrogen was used as carrier gas at a flow rate of 2.5 mL min^{-1} and *n*-hexatriacontane as an internal standard to determine concentrations. To estimate SSTs, we used the $U^{K'}_{37}$ index based on the di- and tri-unsaturated alkenones ratio and converted it into temperature values using the global core top calibration of Müller et al. (1998), with an analytical uncertainty of ±0.5 °C.

4 Chronostratigraphy and age models

One goal of IODP Expedition 339 was always to use the open-ocean records from Site U1385 to establish age models for the contourite sites, which are potentially affected by current sorting and tectonics (Hernández-Molina et al., 2016a) and are too shallow to record a global ocean benthic δ^{18}O signal. So, for contourite sites like IODP Site U1387 the planned approach was to correlate their *G. bulloides* δ^{18}O surface water record with the one of Site U1385 and thus to transfer the U1385 age model(s) to the contourite site, under the assumption that those records would be similar in such a narrow region affected by the same surface water masses. That approach was followed in this study using the high-resolution *G. bulloides* δ^{18}O record (Hodell et al., 2023b) published by Hodell et al. (2023a) as the correlation target for the Site U1387 record. One of the age models of Site U1385 was established by tuning its benthic δ^{18}O record (Hodell et al., 2023a) to the benthic LR04 stack (Lisiecki and Raymo, 2005), whereas an alternative age model applied tuning to the Probstack (Ahn et al., 2017). The age model used throughout this paper for Site U1387 uses the LR04-related ages, although, following Hodell et al. (2023b), Probstack-based ages (Fig. S2) are also provided with the data uploaded to the PANGAEA world data center (Felden et al., 2023). For MIS boundaries, we follow Lisiecki and Raymo (2005) and for MIS substage nomenclature Railsback et al. (2015).

5 Results

5.1 *G. bulloides* δ^{18}O record and chronostratigraphy

Besides the glacial–interglacial cycles of MIS 28 to MIS 18, the *G. bulloides* δ^{18}O record of Site U1387 reveals millennial-scale stadial–interstadial oscillations, especially following the interglacial periods of MIS 25e, MIS 21g, and MIS 19c (Fig. 2a). Notably, an interstadial event occurs within MIS 22 that is also well captured in the Corchia cave δ^{18}O record (Bajo et al., 2020a). Overall, the record mimics the one of Site U1385, facilitating the tuning and age model transference (Figs. 2, S2). The resulting age model for Site U1387 reveals that sedimentation rates were lower during the interglacial intervals dropping to values around 10 cm kyr^{-1} (MIS 19c, MIS 21g), whereas they increased during transitional and glacial periods (Fig. 2c). The same pattern in sedimentation rates is generally observed for the Probstack-based age model (Fig. S2), although age ranges are shifted towards younger ages in the MIS 21 to MIS 28 interval, and there is an interval with higher sedimentation rates in early MIS 26. Both the LR04 and Probstack chronologies diverge significantly from the U–Pb-dated Corchia cave speleothem age model of Bajo et al. (2020a, b) in the interval from early MIS 20 to late MIS 25, whereby the speleothem-based ages greatly change the durations of interglacial MIS 23c and MIS 21g and the timing of Termination X (Figs. S2, 4).

5.2 Planktonic foraminifera fauna

At Site U1387, we found faunal assemblages composed by a mix of species from polar, subpolar, transitional, subtropical, and tropical provinces (Table 1). In total, 16 species were identified (Table 1; Fig. 3). The diversity of the subtropical fauna appears to be diminished due to the absence of *Globoturborotalita tenella*, *Globoturborotalita rubescens*, and *Globorotalia hirsuta*. Although occurring in low percentages, all three species are present in surface and Holocene-aged sediments of the southwestern Portuguese margin and in the Gulf of Cadiz (e.g., Ducassou et al., 2018; Rufino et al., 2022; Salgueiro et al., 2008), and both *Globoturborotalita tenella* and *Globoturborotalita rubescens* have been observed in MIS 19 and younger sediments at Site U1385 (Girone et al., 2023; Martin-Garcia et al., 2015).

Among all species found, only seven have average abundances greater than 2 % over the period studied, i.e., *N. pachyderma*, *N. incompta*, *G. inflata*, *G. ruber* (white), *T. quinqueloba*, *G. bulloides*, and *G. glutinata* (Fig. 3). These seven species are among the top 10 ranked by importance for transfer function models (Jonkers and Kučera, 2019). Two additional species from the top 10 list (*T. sacculifer* and *N. dutertrei*) are present in the samples but with an abundance of less than 2 %, and one (*G. ruber* (pink)) is absent. In summary, the results show an alternation of dominance between cold, transitional, and warm species through MIS 28 to MIS 18, representing changing conditions in the North Atlantic subtropical gyre.

Table 1. Species found at IODP Site U1387 and the respective provinces.

Province	Species
Polar	*Neogloboquadrina pachyderma*
Subpolar	*Neogloboquadrina incompta* *Turborotalita quinqueloba**
Transitional	*Globorotalia inflata** *Globorotalia scitula** *Globigerinita glutinata** *Globigerina bulloides**
Subtropical	*Globigerinella calida* *Globigerinella siphonifera** *Globigerinoides ruber* (white)* *Neogloboquadrina dutertrei* *Globorotalia truncatulinoides** *Globigerina falconensis** *Orbulina universa*
Tropical	*Trilobatus sacculifer** *Globorotalia crassaformis*

* Indicates species associated with the Azores Current by Storz et al. (2009).

In general, the transitional group is the more abundant one, with an average abundance of 40.3 %, followed by the polar–subpolar group, 38.8 %, and finally the tropical–subtropical group, 20.2 % (Fig. 4; Table S1). The transitional group is present throughout the studied interval but exhibits behavior like the tropical–subtropical group, i.e. low percentages, during some events when the polar–subpolar group dominates the assemblage.

Of the 356 samples, 75 screened for % GTS yielded fewer than 20 specimens (24 with 0 specimens), the cut-off criteria defined by Kaiser et al. (2019), making the % GTS values around 974, 959, and 954 ka and in the intervals 923.3–917.8 ka and 893.7–886.8 ka unreliable (Fig. 4b, c). In the earlier part of the record, % GTS increases were less pronounced with three short-term peaks within MIS 28, followed by two peaks during MIS 26 and early MIS 25g. Larger peaks exceeding 80 % GTS occurred between 929.6–927.3 ka, flanking the MIS 22–MIS 21 transition with reliable data centered around 874 and 862 ka and around 823 ka (Fig. 4b).

5.3 Sea surface temperatures

The SSTs from IODP Site U1387 estimated with the planktonic foraminifera assemblage (PF-SST) do not reflect a clear pattern for interglacial–glacial cycles from MIS 28 to MIS 18. Although winter SSTs varied between 0.9 and 19.8 °C and summer SSTs between 4.8 and 24.7 °C (Fig. 5),

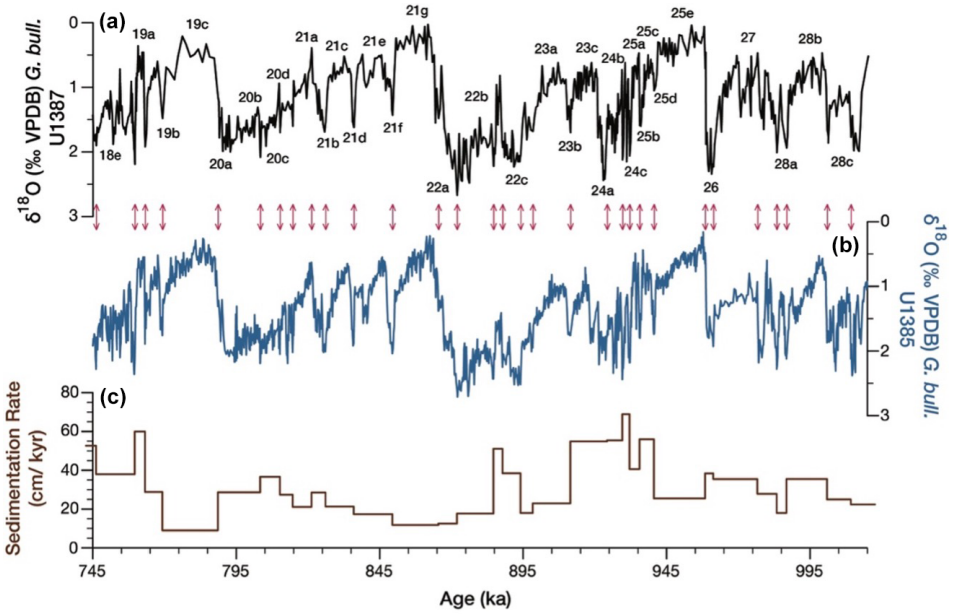

Figure 2. **(a)** δ^{18}O (‰) *G. bulloides* from IODP Site U1387 and Marine Isotopic Stages and substages. **(b)** δ^{18}O (‰) *G. bulloides* from IODP Site U1385 on its LR04-related age model (Hodell et al., 2023b). Arrows between **(a)** and **(b)** indicate the tuning points between the two records. **(c)** Sedimentation rates (cm kyr^{-1}) for IODP Site U1387.

temperatures remained elevated and relative stable during long periods, with an average of 14.3 °C for winter and of 19.4 °C for summer, excluding the extremely cold events. Those conditions were interrupted by short, extremely cold events when the percentage of polar and subpolar species increased (Fig. 4f), and winter SSTs dropped below 5 °C (Fig. 5c). Such events occurred during the glacial MIS and during many MIS substages, associated with stadial climate conditions (e.g., 25b, 23b, 21d, 21b, 19b). The error (1σ) for the winter SSTs ranges from 0.2 to 4.8 °C and for the summer SSTs from 0.3 to 5.4 °C, with the larger errors associated with those samples with lower similarity values (Fig. 5). The similarity between the respective Site U1387 sample and the selected 10 modern analog database samples used to estimate the temperatures is generally above 0.9. Some samples, often associated with extreme cold events, have a lower similarity between 0.9 and 0.75 (Fig. 5d). At these specific lower similarity samples, we observe a small contribution of "warm" species in a dominantly "cold" assemblage, leading to a non-analog situation. The species mix and consequently reduced similarity could be linked to bioturbation and/or current transport in those contourite layers (Expedition 339 Scientists, 2013) or to the presence of *N. pachyderma* variants with different temperature affinities (see discussion in Sect. 6.3).

The alkenone SST ($U^{k'}_{37}$-SST) record with annual temperatures ranging from 9.05 to 23.3 °C shows a clear glacial–interglacial cycle pattern (Fig. 6). Despite the differences in amplitudes, both techniques registered the extreme cold events contemporaneously, corroborating the interpretation of these results. The coldest period was recorded at the end of MIS 22 between 870.3 and 864.3 ka. During this period, we recorded the highest percentage of *N. pachyderma* (75.5 %) and the lowest temperatures with PF-SST of 4.8 °C for summer and 0.9 °C for winter and $U^{k'}_{37}$-SST of 9.05 °C.

6 Discussion

6.1 Persisting subtropical gyre influence

The strong influence of the AzC in the region is evident through the comparison between the modern planktonic foraminifera assemblage composition (Salgueiro et al., 2008; Rufino et al., 2022) and the reconstructed assemblages from Iberian margin sediments (Girone et al., 2023; Martin-Garcia et al., 2015; Salgueiro et al., 2010; Voelker et al., 2009). During the EMPT, the interglacial and interstadial stages recorded the warmest temperatures, associated with higher percentages of tropical, subtropical and transitional species (Figs. 3; 4d, e). According to Salgueiro et al. (2008), high abundances of *G. ruber* (white), *T. sacculifer*, and *G. inflata* at the Iberian margin are indicative of the presence of the AzC's eastern branch (AzC factor; Fig. 6d), whereas Storz et al. (2009) associated a much larger species group with the AzC within the subtropical gyre (Table 1). The relatively warm SSTs depicted throughout most of the records, i.e., summer PF-SST within a range of 21 to 24.7 °C and winter PF-SST within 15 to 19.8 °C, are associated with the "AzC fauna" that include species from the transitional and subtropical provinces (Salgueiro et al., 2008; Storz et al., 2009); so,

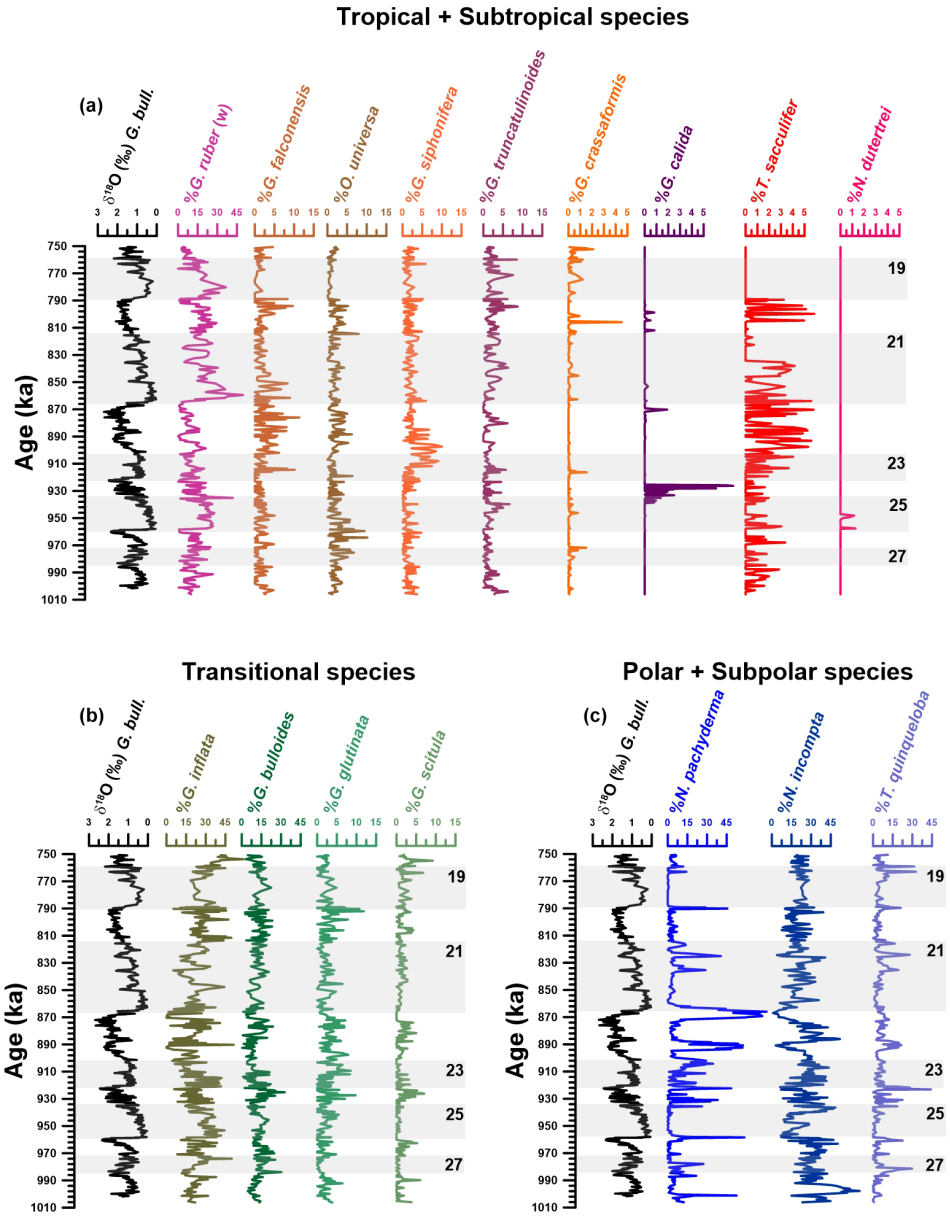

Figure 3. Planktonic foraminifera assemblage from IODP Site U1387. δ^{18}O *G. bulloides* record (‰ VPDB) (black) provided in all three panels as stratigraphic reference. **(a)** Abundance (%) of tropical species (*Trilobatus sacculifer*, *Globorotalia crassaformis*) and subtropical species (*Globigerinella siphonifera*, *Globigerinoides ruber* (white), *Neogloboquadrina dutertrei*, *Globigerinella calida*, *Orbulina universa*, *Globigerina falconensis*, *Globorotalia truncatulinoides*). **(b)** Abundance (%) of transitional species (*Globorotalia inflata*, *Globorotalia scitula*, *Globigerinita glutinata*, *Globigerina bulloides*). **(c)** Abundance (%) of polar species (*Neogloboquadrina pachyderma*) and subpolar species (*Neogloboquadrina incompta*; *Turborotalita quinqueloba*). Grey bars mark odd-numbered MISs, which include the interglacial periods. Note the differing *y*-axis scales.

we interpret those periods with combined increased abundances of tropical, subtropical, and transitional species and with values for the AzC factor above 30 % (Fig. 6d) as being under AzC and thus subtropical gyre influence.

The persistent abundance of *N. incompta* (Fig. 3), slightly above the mean value of 18 % observed in the surface sediments (Salgueiro et al., 2008), also points to Portugal Current contributions to the prevailing surface waters as it is a main contributor to the Portugal Current factor (Salgueiro et al., 2008). Whereas higher abundances of *G. bulloides* during the EMPT interglacial periods at western Iberian Margin Site U1391 (Fig. 1b) are interpreted as high productivity upwelling periods (Singh et al., 2015), the same is not observed at Site U1387. Here the percentages of *G. bulloides* gen-

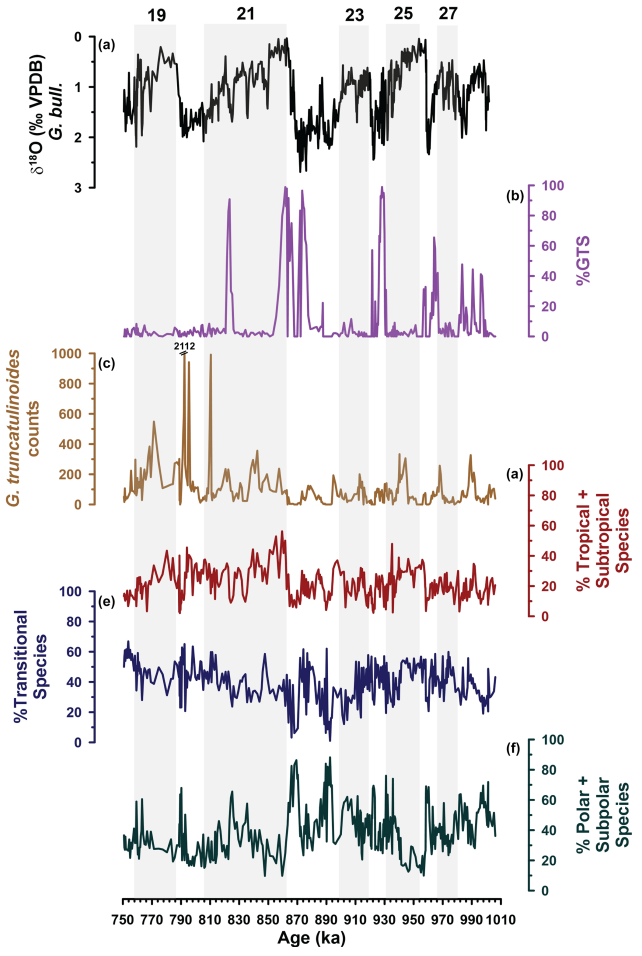

Figure 4. Site U1387 faunal provinces and *Globorotalia truncatulinoides* results. **(a)** δ^{18}O (‰) *G. bulloides*. **(b)** *G. truncatulinoides* coiling ratio expressed as % of *G. truncatulinoides* (sinistral), showing all the data and thus including not reliable points that are based on fewer than 20 specimens counted (e.g., during the MIS 22–MIS 21 transition). **(c)** Number of *G. truncatulinoides* specimens counted in the fraction $> 250\,\mu m$ and used to calculate the coiling ratio in **(c)**. **(d)** Abundance (%) summed up for tropical and subtropical species. **(e)** Abundance (%) of transitional species. **(f)** Abundance (%) of polar and subpolar species. Grey bars mark the odd-numbered MISs.

erally remain below the local surface sediment mean value of 34 % (Salgueiro et al., 2008) with no distinct glacial–interglacial variations, although percentages increased during glacial MIS 24 and MIS 22 (Fig. 3). We interpret the *G. bulloides* pattern at Site U1387 more as a temperature response, with limited influence of waters upwelled in the major upwelling cell off Cape St. Vincent (Fig. 1b) and advected towards Site U1387. Nevertheless, the sporadic presence of *Chaetoceros* resting spores (diatoms) within interglacial MIS 25e and MIS 28b (called MIS 27b in cited reference) documents some influence of seasonal upwelling at Site U1387 (Ventura et al., 2017). Interestingly, the rare occurrences of planktonic foraminifera *N. dutertrei* in MIS 25e (Fig. 3) coincide with the presence of the large-diameter marine diatom species *Coscinodiscus asteromphalus* (Ventura et al., 2017), which can form large blooms and would thus be an ideal food source for *N. dutertrei* (Schiebel and Hemleben, 2017).

The $U^{k'}_{37}$-SST data show similar patterns to the PF-SSTs with relatively stable temperatures during interglacial and interstadial substages (Fig. 6), although some intra-interglacial variability is observed (see discussion below). In contrast to the PF-SSTs, the $U^{k'}_{37}$-SSTs reveal a clear cooling trend from the respective interglacial optimum to the subsequent glacial maximum. This different pattern cannot solely be attributed to the $U^{k'}_{37}$-SSTs reflecting annual mean temperatures instead of seasonal ones like the PF-SSTs. During the Last Glacial Maximum, the tropical and subtropical regions cooled (MARGO Project Members, 2009; Osman et al., 2021; Tierney et al., 2020); therefore we should also expect climatic response and cooling in those regions during the EMPT glacial cycles, conforming with the $U^{k'}_{37}$-SST record of Site U1387 and other global records (McClymont et al., 2013; Naafs et al., 2013; Rodrigues et al., 2017). The difference in the reconstructed SST pattern must, therefore, be caused by the planktonic foraminifera fauna itself. While not obvious in the reconstructed PF-SSTs, a decline in the abundance of the AzC species (Fig. 6d), largely driven by declining *G. ruber* (white) contributions (Fig. 3), and a contemporary increase in Portugal Current-associated species (*G. inflata*, *N. incompta*; Fig. 3) are evident in all those interglacial–glacial cycles, also pointing to some cooling on the zooplankton level. However, the AzC factor fauna (Fig. 6d) and other species linked to subtropical gyre waters (Fig. 4d) retain relative high percentages; therefore the transfer function is looking for modern analogs in relative warm waters to estimate the EMPT faunal-derived SSTs. Thus, due to the fauna being too similar to modern subtropical gyre assemblages (Fig. 5d), the estimated PF-SSTs at Site U1387 appear too warm and do not reflect the global cooling, also expected for the North Atlantic subtropical gyre, during the transitions from the glacial inception to the glacial maximum, at least for the glacial cycles covered by this study. The same pattern is also evident for the PF-SSTs obtained for IODP Site U1385 (Martin-Garcia et al., 2015), which also remained warmer than the corresponding $U^{k'}_{37}$-SSTs (Rodrigues et al., 2017).

Site U1387 $U^{k'}_{37}$-SSTs are $\sim 2.5\,^{\circ}C$ warmer than the $U^{k'}_{37}$-SSTs of IODP Site U1385 on the southwestern Portuguese margin (Fig. 1b), but the overall trends are the same (Fig. 6c). A similar temperature difference between both sites is also visible for the PF-SST reconstructions for MIS 21 to MIS 19 (i.e., within the interval the records overlap; Martin-Garcia et al., 2015), although the Site U1385 PF-SSTs were obtained using the artificial neural network method and the original MARGO modern analog database from Kučera et al. (2005). We attribute the temperature gradient to a stronger AzC influence at Site U1387, whereas Site U1385 is more affected

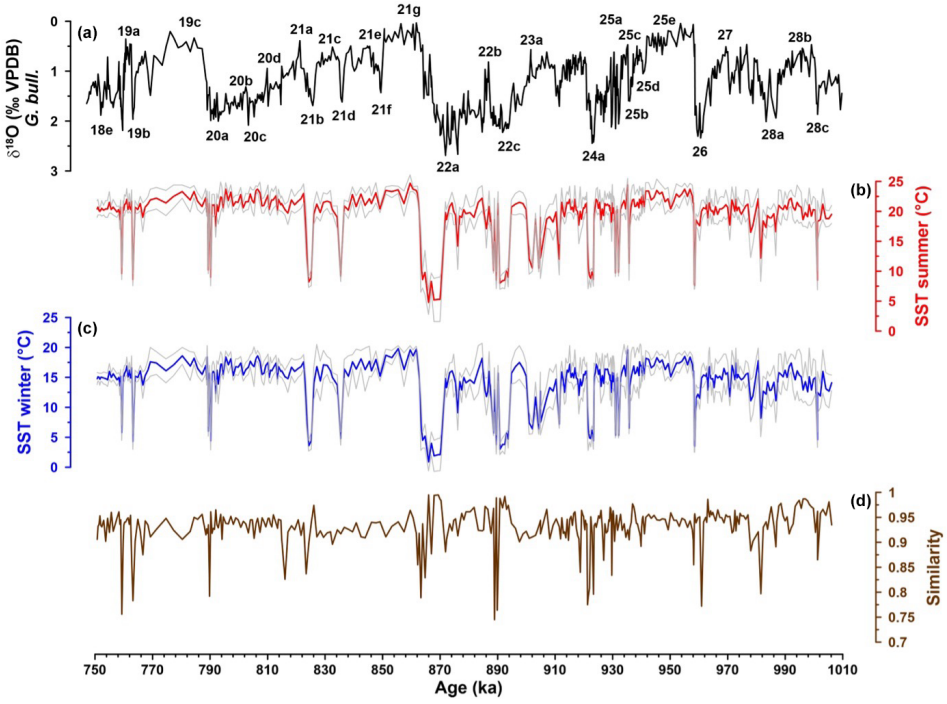

Figure 5. IODP Site U1387 planktonic-foraminifera-derived SST records **(a)** δ^{18}O *G. bulloides* (‰ VPDB) with numbered Marine Isotopic Stages and substages. **(b)** Summer SSTs (°C) with standard deviation (1σ). **(c)** Winter SSTs (°C) with standard deviation (1σ). **(d)** Similarity to modern analogs used to calculate the SSTs.

by the cooler Portugal Current waters (modern annual mean of 16.1 °C) and by seasonal upwelling (Fig. 1b).

In the Gulf of Cadiz, the summer PF-SSTs and $U^{k'}_{37}$-SSTs reconstructed for the EMPT interglacials were as warm as or slightly warmer than the current interglacial SST (∼ 22 °C; Salgueiro et al., 2014) in the case of the warmer interglacials, i.e., MIS 19c, MIS 21g, and MIS 25e, and 1.5 °C cooler during MIS 23c and MIS 27, which is only observed in the PF-SSTs (Fig. 6b). However, neither of those interglacial periods experienced surface waters as warm as during the Early Pleistocene interglacial MIS 47, when $U^{k'}_{37}$-SSTs remained above 24 °C and subtropical planktonic foraminifera abundance mostly above 40 % (Voelker et al., 2022). The warmest EMPT interglacial was MIS 21g, supported by high contributions of the subtropical–tropical fauna of up to 56.3 % vs. 45.5 % during MIS 19c and 38 % during MIS 25e (Fig. 4), even though MIS 25e received the higher amount of insolation (Rodrigues et al., 2017). The maximum percentages are comparable to those observed during MIS 47 (generally exceeding 40 % and reaching up to 66.8 %), although periods with such high contributions were much shorter during the EMPT interglacials. Much of the subtropical–tropical fauna abundance is driven by the contribution of *G. ruber* (white) (Fig. 3), which can attribute nearly half of the overall percentage. *G. ruber* (white) added less to the MIS 23c fauna (11 %), but this interglacial had a unique fauna due to the higher influence of the subtropical species *G. siphonifera* (2.85 %) (Fig. 3) that persisted into MIS 23a when PF-SSTs became less stable, caused by the mixture of planktonic foraminifera provinces (including subpolar and polar species).

Intra-interglacial SST variability is observed during several of the interglacials because a cooling event was recorded in both SST reconstructions during MIS 21g, MIS 23c, and MIS 27, leading to a three-phased SST evolution, although the timing of the cooling event within the interglacial period varied (Fig. 6). The PF-SSTs also documented such a cooling event for MIS 25e, where it occurred prior to the increase in the $U^{k'}_{37}$-SSTs in the younger phase of the interglacial. As such, the MIS 25e $U^{k'}_{37}$-SST pattern mimicked the one of MIS 11c on the Portuguese margin (Rodrigues et al., 2011) and in the mid-latitudinal North Atlantic (Stein et al., 2009), though on a shorter timescale. For both MIS 25e (Ventura et al., 2017) and MIS 11c on the western Portuguese margin (Rodrigues et al., 2011), the early phase of the interglacial is associated with upwelling activity and thus the (temporary) presence of cooler surface waters.

Recently, Barker et al. (2021) proposed treating MIS 28 as a "missed" interglacial, and we therefore include it in our comparison. The summer PF-SST and $U^{k'}_{37}$-SST records of Site U1387 would support such a notion. Specifically, during the interstadial MIS 28b, warm PF-SSTs and $U^{k'}_{37}$-SSTs of 19.6 and 21.1 °C , respectively, and considerable contributions of the AzC factor fauna suggest categorizing this period as an interglacial (Fig. 6).

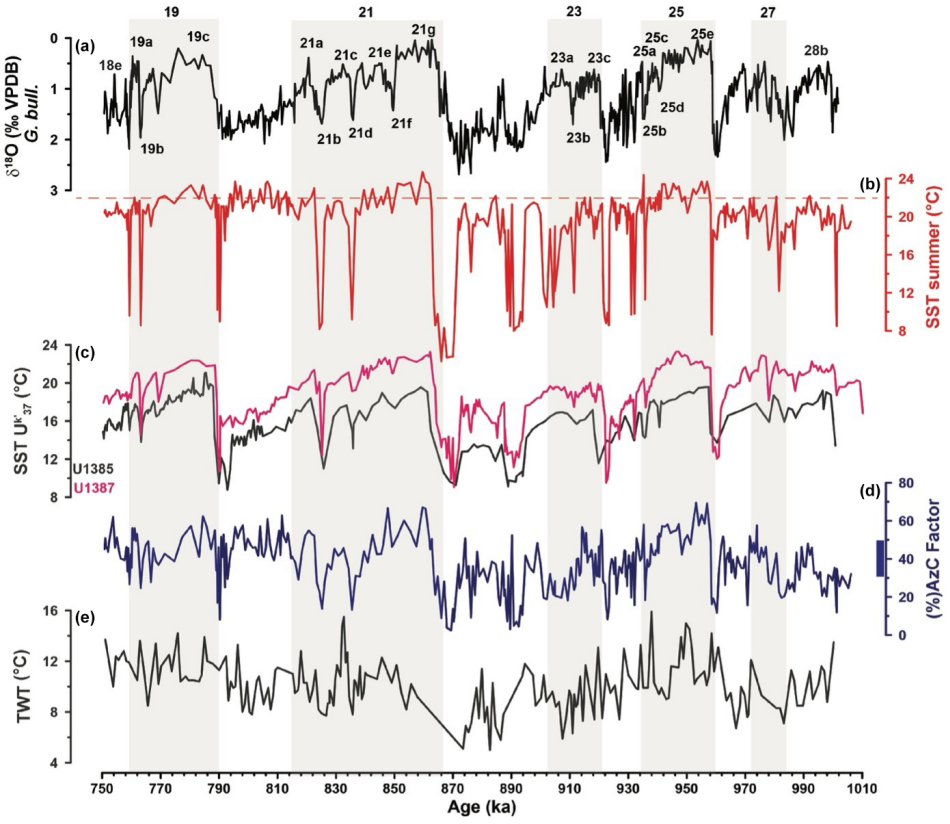

Figure 6. Comparing Site U1387 and Site U1385 temperature records. **(a)** δ^{18}O *G. bulloides* record of IODP Site U1387 (‰ VPDB) with the MIS and substages indicated. **(b)** Planktonic foraminifera summer SSTs (°C) from Site U1387, with the dashed line marking the Late Holocene level of 22 °C. **(c)** Alkenone-derived SST record of IODP Site U1387 (magenta; Bajo et al., 2020a, and this study) in comparison to the Site U1385 record (dark grey; Rodrigues et al., 2017; Rodrigues et al., 2020). **(d)** The Azores Current factor (%) from IODP Site U1387, with the bar next to the scale indicating the modern range in Gulf of Cadiz surface samples (Salgueiro et al., 2008). **(e)** Thermocline water temperature (TWT) at Site U1385 (Bahr et al., 2018; Bahr et al., 2017). Grey bars mark the odd-numbered MISs.

Millennial-scale variability in the form of stadial–interstadial oscillations is observed in our records, in accordance with evidence from other North Atlantic sites, evidencing significant modifications in the North Atlantic's thermohaline circulation, the expansion of continental ice sheets and sea ice, and the atmospheric circulation (e.g., Barker et al., 2021; Billups and Scheinwald, 2014; Hernández-Almeida et al., 2015; Hodell and Channell, 2016; Hodell et al., 2015, 2023a; Sun et al., 2021; Rodrigues et al., 2017). At Site U1387, one of the most dynamic periods was the interval between MIS 25 and MIS 20, which points to highly variable surface water conditions in the northern subtropical gyre region, in accordance with evidence from DSDP Site 607 and IODP Site U1313 (Marino et al., 2008; Naafs et al., 2013). Here, we focus on the interstadial periods, with the stadials being discussed later in Sect. 6.3. At Site U1387, the interstadials recorded high mean summer PF-SSTs (20.8 °C), similar to the $U^{k'}_{37}$-SSTs (20.0 °C), and a mean winter PF-SSTs of 15.7 °C. The warmest interstadial according to the summer PF-SSTs was MIS 21e with 23.1 °C, whereas the cooler one reached around 19.9 °C (Figs. 5, 6). The interstadials had variable durations, with MIS 22b being the longest period with ∼ 16 kyr and MIS 20b the shortest with ∼ 1.5 kyr. The interstadial MIS 22b, occurring during the middle of the glacial MIS 22 and thus within the 900 ka event period, had a summer PF-SSTs in the general range of 19–21 °C, with the $U^{k'}_{37}$-SSTs being slightly cooler in the 17–18 °C range (Fig. 6). During the interstadials of MIS 23, MIS 22, MIS 21, and MIS 20, noteworthy occurrences of the tropical, surface-dwelling species *T. sacculifer* are observed, with 1.9 % on average but increasing to 2.9 % during MIS 21c (Fig. 3). The periods also registered the greatest abundances of the subtropical species *G. falconensis* (average 2.7 %), increasing to 4.6 % during the interstadial MIS 20b. Those indicator species, together with the higher AzC factor fauna abundance (Fig. 6d), confirm the prevailing subtropical gyre water influence and a strong presence of the AzC at the southern Portuguese margin during the interstadials, in accordance with previous observations on the southwestern margin (Girone et al., 2023; Martin-Garcia et al., 2015; Singh et al., 2015). Those warm surface waters were subducted into the thermocline levels and the subtropical North Atlantic Central Wa-

ter (Bahr et al., 2018). Bahr et al. (2018) link an intensified AzC, coupled to a strong Mediterranean Outflow Water, to their warmer thermocline water temperatures, which conforms with our SST and faunal evidence (e.g., MIS 22b, MIS 21c, MIS 19a) (Fig. 6).

6.2 *G. truncatulinoides* evidence for subtropical gyre state

G. truncatulinoides is a planktonic foraminifera species that prefers relatively warm, nutrient-rich waters such as at the subtropical gyre margins (Ujiié et al., 2010; Rufino et al., 2022). According to Kaiser et al. (2019) and Feldmeijer et al. (2015), the sinistral variant dominates North Atlantic regions with a deep permanent thermocline, such as the central subtropical gyre. Its presence at mid-latitudinal North Atlantic sites, especially during glacial periods, can indicate the northward flux of subtropical waters and thus the position of the gyre's northern boundary (Kaiser et al., 2019). In contrast, *G. truncatulinoides* (dextral) dominates in the Atlantic's tropical waters and in the cooler subtropical and transitional waters encountered in the NE Atlantic north of 40° N. High percentages of that variant have been interpreted as reflecting higher contributions of North Equatorial Current and Antilles Current waters (Fig. 1) to the Gulf Stream and thus enhanced westward and northward transport along the western boundary of the subtropical gyre and into its central regions, corresponding with an enhanced gyre circulation overall (Billups et al., 2020).

The percentage contributions of *G. truncatulinoides* to the Site U1387 EMPT fauna themselves (Fig. 3) are in the same range as those observed in surface sediments along the western Iberian margin, in the Gulf of Cadiz and the eastern boundary current region off NW Africa (Salgueiro et al., 2008; Rufino et al., 2022). Concerning the coiling direction, the dextral variant dominates during much of the interval, conforming with other North Atlantic sites in gyre boundary locations (Kaiser et al., 2019) (Fig. 7). The foremost characteristics of the % GTS record are, however, increased contributions of the left coiling variant during MIS 28, MIS 26, and MIS 24 and at the end of stadial MIS 21b and two maxima bracketing the terminal stadial event of Termination X (Fig. 7c). Many of those % GTS peaks have counterparts at Site 607 in the northern subtropical gyre (Fig. 7e), where those maxima imply the vicinity of the gyre's northern boundary (Kaiser et al., 2019) and thus a gyre northward expansion not much different to today, in agreement with the relative warm subsurface temperatures reconstructed at the same location (Catunda et al., 2021). The Site U1387 % GTS increases during MIS 28 and MIS 24 and following the terminal stadial event of Termination XII (MIS 26/MIS 25) have no counterparts at Site 607 (Kaiser et al., 2019), at least within the temporal resolution and age model constraints (Fig. 7). With the exception of the event during MIS 24, those % GTS peaks reached mid-range values (30 %–65 %), similar to those observed in the surface sediments along the southwestern and southern Portuguese margin. So, conditions during those periods were probably comparable to modern conditions with substantial AzC influence and the warm water body of the subtropical North Atlantic Central Water extending down to 250–300 m in the vicinity of Site U1387 (Voelker et al., 2015a, b). With the exception of the early MIS 28 peaks, such a scenario is supported by the AzC related faunal contributions at Site U1387 (Fig. 6d), although, within the age constraints, no related warming events are seen in the Site U1385 thermocline temperature record (Fig. 6e).

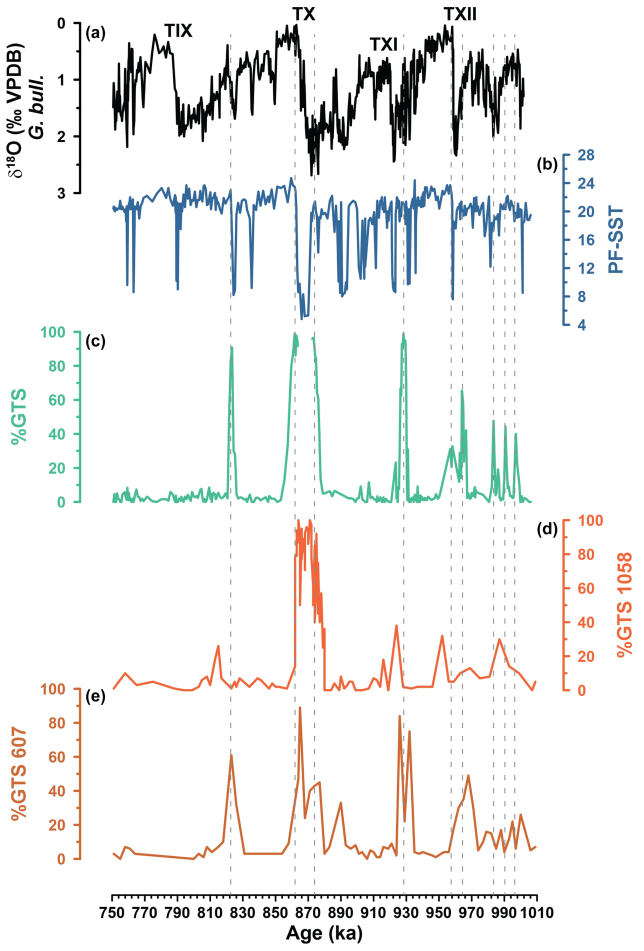

Figure 7. Subtropical gyre intensification episodes. **(a)** δ^{18}O (‰) *G. bulloides* from IODP Site U1387. **(b)** Summer PF-SST from IODP Site U1387. **(c)** Coiling ratio (%) of planktonic foraminifera *G. truncatulinoides* (sinistral) from IODP Site U1387 (only showing reliable data points based on counts of ≥ 20 specimens). **(d)** Coiling ratio (%) of planktonic foraminifera *G. truncatulinoides* (sinistral) from ODP Site 1058 (Kaiser et al., 2019). **(e)** Coiling ratio (%) of planktonic foraminifera *G. truncatulinoides* (sinistral) from DSDP Site 607 (Kaiser et al., 2019). Dashed lines mark peaks of U1387 % GTS maxima. Terminations are indicated by the letter T and the respective Latin numerical.

The most prominent feature in the % GTS records of Sites U1387, 607, and 1058 is the period from MIS 22a to MIS 21g, when % GTS temporarily reached values between 80 % and 100 % (Fig. 7). At ODP Site 1058 at the western boundary/Gulf Stream, the feature is one long-lasting (∼ 20 kyr) peak, whereas at DSDP Site 607 a double peak is observed. At Site U1387, only the onset and ending of the broader ODP Site 1058 peak are recorded because during the extreme cold event, *G. truncatulinoides* disappeared or nearly disappeared from the fauna, indicating the absence of a warm subsurface layer. Based on their data from Sites 1058 and 607, Kaiser et al. (2019) posited that the North Atlantic's subtropical gyre expanded as far north as 41° N (or further) during glacial MIS 22a and that its circulation was more vigorous than during the Last Glacial Maximum (at least based on the % GTS evidence, which, for the Last Glacial Maximum, is not in agreement with the new results from Wharton et al., 2024). This scenario agrees with the warm subsurface temperatures reconstructed at IODP Site U1313 during MIS 22a (Catunda et al., 2021), which were not much cooler than interglacial levels and indicate an expanded layer of subtropical gyre waters. The Site U1387 records (% GTS, AzC factor; Figs. 6d, 7c) now corroborate that the well-developed subtropical gyre extended to the basin's eastern margin but only during the restricted periods of 877–873 ka and 864–857 ka. During the terminal stadial event of Termination X, the subtropical gyre contracted in the north and east, leading to the % GTS minimum at Site 607 and temporary absence of the species at Site U1387, whereas its western boundary remained near the position of Site 1058 (Kaiser et al., 2019). When the subarctic front receded northward after the terminal stadial event of Termination X, the subtropical gyre expanded again into its modern configuration as evidenced by the % GTS maxima at Site 607 and U1387 (Fig. 7). This facilitated subtropical water transport to the north and enabled deep-water convection in the North Atlantic to penetrate once more into depths below 3800 m (Site U1308; Fig. 8g) (Hodell and Channell, 2016; Hodell et al., 2023a; Kaiser et al., 2019), thus the establishment of interglacial conditions.

The other two pronounced % GTS peaks at Site U1387, i.e., during MIS 24 and late MIS 21, occurred at the onset of an interstadial that followed a stadial with an extreme cooling event (Fig. 7), when the AzC-related fauna was reduced (Fig. 6c) and subtropical gyre water influence therefore diminished (Fig. 7). So, similar to the sequence of events during the onset of MIS 21g, we interpret the % GTS signal as reflecting a well-developed subtropical gyre expanding once more to the Portuguese margin after the subarctic front receded northward. Both % GTS maxima were associated with an increased AzC influence at Site U1387 (Fig. 6c), an expanded warm water layer at DSDP Site 607 (% GTS; Fig. 7e) and IODP Site U1313 (subsurface temperature; Catunda et al., 2021), and a deeper AMOC with well-ventilated NADW reaching depths > 3800 m (Fig. 8g; Hodell and Channell, 2016). To account for the high % GTS values, in comparison for example to the smaller % GTS increase at the onset of MIS 25e with an overall similar sequence of climate signals, we postulate that the eastern boundary circulation might have been more vigorous for a short period during the eastward expansion of the gyre.

6.3 The extreme cold events

Site U1387 recorded several short stadial events (∼ 2 kyr) following the glacial inception and terminal stadial events, with winter PF-SSTs dropping to ∼ 5 °C during MIS 24a or even to freezing temperatures of 0 °C during MIS 22a (Figs. 5, 8b). The $U^{k'}_{37}$-SSTs during those terminal stadial events also reflect extremely low temperatures, but these only reach 10 °C during MIS 22a and MIS 24a (Fig. 6c). The southern position of the subarctic/Arctic front during those stadial periods (Martin-Garcia et al., 2015; Rodrigues et al., 2017) facilitated the presence of the polar species *N. pachyderma* , which reached between 80 % (MIS 22a) and 50 % (MIS 24a) (Fig. 8c), as well as a general increase in the number of polar and subpolar species (Fig. 8d). The high percentages of *N. pachyderma* are much higher than those observed during the Heinrich events of the last glacial cycle in the Gulf of Cadiz (< 20 %) and also exceed those observed in general on the southwestern Portuguese margin during the last 400 kyr (< 40 %) (Salgueiro et al., 2014, 2010; Singh et al., 2023; Voelker and de Abreu, 2011). They drive the extremely cold SST estimated for the PF-SST, which appears to introduce a "cold bias" for the winter PF-SST, which is much colder than the (annual mean) $U^{k'}_{37}$-SSTs (Figs. 6, 8). The *N. pachyderma* morphotypes (Fig. S1) are similar to those found today in the subpolar to polar North Atlantic and those observed in contemporary "Middle" Pleistocene sediments in the Alboran Sea (western Mediterranean Sea) (Serrano and Guerra-Merchán, 2012). Although *N. pachyderma* adapted to the colder, polar conditions 1100–1000 kyr ago (Huber et al., 2000; Kučera, 2007), thereby establishing the modern polar *N. pachyderma* variant (genotype Ia), a recent review of genetic diversity in planktonic foraminifera from the modern global ocean (Morard et al., 2024) revealed that other *N. pachyderma* genotypes only occur in lower- to mid-latitudinal waters of the Atlantic (e.g., Va, VIa), whereby genotype VIa is well established in the mid-latitudinal North Atlantic, especially in the AzC region, and the Mediterranean Sea. Serrano and Guerra-Merchán (2012) postulated that their Early Pleistocene *Neogloboquadrina* specimens from the Alboran Sea might include two groups with different temperature affinities, one being the modern polar variant and the other living in warmer waters and/or upwelling conditions. Their observations indicate that the mid-latitudinal North Atlantic genotype VIa or a precursor of it might have already been present in the Early Pleistocene. As it is difficult to distinguish between the genotypes based on morphology, it is possible that the Site U1387 EMPT *N. pachyderma* specimens include both the polar and the mid-latitudinal, warmer

water affinity variants. Presence of a warmer water variant would agree with the low but noticeable contemporary presence of various subtropical species and of tropical species *T. sacculifer* in the Site U1387 fauna (Figs. 3, 4d) that hint at some AzC and subtropical gyre influence. This is especially true for MIS 22, when such subtropical water contributions would be consistent with the relative northern expansion of the subtropical gyre (Catunda et al., 2021; Kaiser et al., 2019). Because the modern analog technique used to calculate the PF-SST relies on the percentage contributions of *N. pachyderma* to the total fauna it looks for modern analogs in the Nordic seas and Labrador Sea and therefore overestimates the cooling if the *% N. pachyderma* values include relevant contributions of a warm water variant or where that variant dominates. So, for the interpretation of the cold stadial events, we give more weight to those events where PF-SSTs and $U^{k'}_{37}$-SSTs show contemporary cooling and caution that some of the extreme cold PF-SSTs might be overestimated.

The terminal stadial events (Fig. 8) are all clearly marked in the PF-SSTs and $U^{k'}_{37}$-SSTs record with extreme cooling. The Termination X event (MIS 22a) lasted the longest (6 kyr) and was the coldest, recording the with lowest SSTs of the whole study interval. In contrast to the southwestern Portuguese margin records from Site U1385 (Girone et al., 2023; Rodrigues et al., 2017), southward incursion of cold surface waters to Site U1387 during Termination IX was much more limited, as indicated by the diminished cooling in regard to amplitude and duration. When compared to the others, an atypical terminal stadial event occurred at the end of MIS 28a with low *N. pachyderma* abundances (20 %) and relatively warm PF-SST (10 °C) (Fig. 8). The event presents, however, an assemblage dominated by polar and subpolar species (60 %) and evidence of ice-rafting at ODP Site 980 in the subpolar North Atlantic (Fig. 8f) (Wright and Flower, 2002). All terminal stadial events recorded at Site U1387 coincided with ice rafting and melting icebergs in the North Atlantic (Fig. 8e, f) (Hodell and Channell, 2016; Marino et al., 2011; Rodrigues et al., 2017; Wright and Flower, 2002) and a related strong reduction of the AMOC depth, as evidenced by the presence of AABW (low benthic δ^{13}C values) in water depths normally occupied by NADW at mid-latitudinal North Atlantic sites from water depths > 2500 m (e.g., IODP Sites U1314, U1308, and U1385) (Fig. 8g) (Hernández-Almeida et al., 2015; Hodell and Channell, 2016; Hodell et al., 2023a). The Site U1387 records, therefore, provide further evidence for an extreme contraction of the subtropical gyre in the eastern North Atlantic during those events and indicate that the subarctic front advanced much further south during those events than during the Heinrich events of the last glacial cycle or any terminal stadial events of the last 400 kyr, as already previously suggested by Rodrigues et al. (2017).

In addition to the terminal stadial events, stadial events occurred during MIS 24c, MIS 23b, MIS 21d, MIS 21b, MIS 19b, and MIS 18e with similar environmental characteristics (Fig. 8). Although those periods presented lower *% N. pachyderma* between 20 % during MIS 18e and 40 % during MIS 24c, the assemblages were dominated by polar and subpolar species (60 %–80 %), resulting in very cold winter PF-SSTs. The transition to the glacial maximum of MIS 24 was marked by three stadial–interstadial oscillations, with the first two occurring early on and with only 2 kyr separating them. The last stadial was a little cooler (4.9 °C) but was associated with a strong increase in *N. pachyderma* abundance (50 %) and high amounts of IRD (80 %) and reworked coccoliths (90 %) in the subpolar North Atlantic at the ODP Site 980 (Marino et al., 2011; Wright and Flower, 2002) (Fig. 8). This evidence, combined with the lower $U^{k'}_{37}$-SST (10 °C) at Site U1387 and the presence of freshwater input at Site U1385 (Rodrigues et al., 2017), indicates a strong southward displacement of the subarctic front also during this event. The cold events in MIS 23b, MIS 21b, and MIS 18e were associated with hardly any cooling in the $U^{k'}_{37}$-SSTs (Fig. 6), representing potential cases of cold bias in the PF-SSTs.

The transition between MIS 23 and MIS 22 initiated the 900 ka event. Cooler temperatures during MIS 23 could lead to an abrupt increase in Antarctic ice volume and thus lowering of the sea level to 120 m below present (Elderfield et al., 2012). The lower sea level permitted the advance of marine-based ice sheets around the North Atlantic with impacts on ice-rafting and subarctic front movements (Hodell and Channell, 2016). At Site U1387, those background conditions resulted in a cooling event during MIS 23a, which is clearly visible in the planktonic foraminifera records but not the $U^{k'}_{37}$-SST records of either Site U1387 or Site U1385 (Figs. 4, 6, 8). It is, however, contemporary with a short cooling in the subtropical gyre's subsurface waters at Site U1313 (Catunda et al., 2021). The cooling trend initiated with this event culminated in the first, prolonged period of extreme cold conditions during MIS22c at Site U1387 (Figs. 6, 8). In the mid-latitudinal North Atlantic, ice rafting and iceberg melting (Hodell and Channell, 2016; Marino et al., 2011; Wright and Flower, 2002) led to freshening of the surface waters, even as far south as Site U1385 (Fig. 8e) (Rodrigues et al., 2017), and subsequently to a reduction in the AMOC depth, as evidenced by the benthic δ^{13}C records of mid-latitudinal North Atlantic sites from water depths > 2100 m (e.g., ODP Site 980/981, IODP Sites U1314, U1308, and U1385) (Fig. 8g) (Hernández-Almeida et al., 2015; Hodell and Channell, 2016; Hodell et al., 2023a; Wright and Flower, 2002). The associated contraction of the subtropical gyre is also reflected in the subsurface waters at Site U1313 cooling by 2 °C to the range of 4 °C (Catunda et al., 2021), a cooling that is not seen during MIS 22a when the subtropical gyre was stronger (Kaiser et al., 2019).

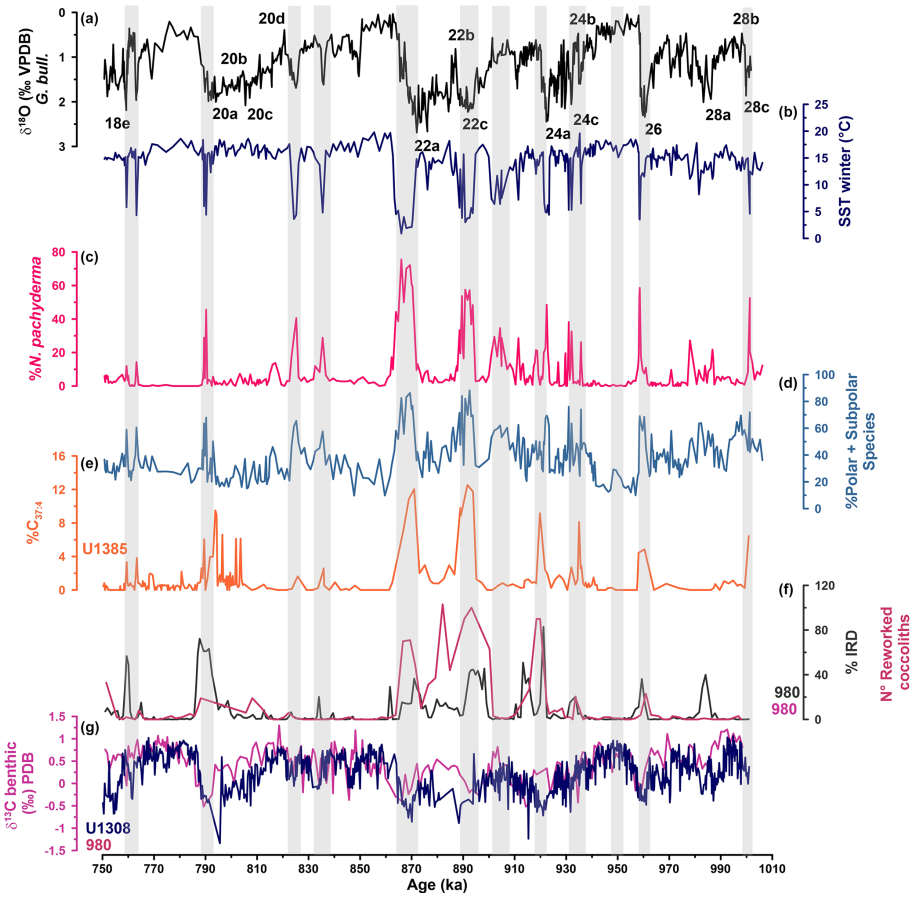

Figure 8. The extreme cold events. **(a)** IODP Site U1387 *G. bulloides* δ^{18}O (‰ VPDB) record with MIS and substages. **(b)** Winter PF-SST (°C) from IODP Site U1387. **(c)** Abundance (%) of the planktonic foraminifera *N. pachyderma* from IODP Site U1387. **(d)** Abundance (%) of polar and subpolar species at IODP Site U1387. **(e)** %$C_{37:4}$ freshwater indicator from IODP Site U1385 (Rodrigues et al., 2017). **(f)** Number of reworked coccoliths (Marino et al., 2011) and abundance (%) of ice-rafted debris from ODP Site 980 (Wright and Flower, 2002). **(g)** δ^{13}C benthic foraminifera (‰ VPDB) (magenta line) from ODP Site 980 (Wright and Flower, 2002), and δ^{13}C benthic foraminifera (‰) (dark-blue line) from IODP Site U1308 (Hodell and Channell, 2016). Grey bars mark cold events.

7 Conclusions

The planktonic foraminifera faunal and SST records of IODP Site U1387 revealed that subtropical gyre waters, especially those related to the AzC, greatly influenced the Gulf of Cadiz during the EMPT interval from MIS 28 to MIS 18, even during the transitions to full glacial conditions following the glacial inception. The planktonic foraminifera fauna includes species from all four provinces, with the subpolar and polar species dominating during the extreme cold events, in particular the terminal stadial events. The faunal diversity differed slightly from the Holocene, a topic of which implications for ecosystem state and restoration efforts in the region will be explored further in the future. Interglacial periods and several of the interstadials experienced SST as warm as or slightly warmer than today and registered persistent AzC influence. The warmest interglacial period was MIS 21g and the coolest, as to be expected from the global climate state, MIS 23. MIS 23 exhibited a particular subtropical planktonic foraminifera fauna, which, in contrast to the other interglacials, included a lesser contribution of *G. ruber* white but higher ones of *G. falconensis* and *G. siphonifera*. Interestingly, the tropical species *T. sacculifer* was present in low percentages throughout MIS 23 and even glacial MIS 22, which included the two periods with the coldest SST of the studied time interval.

Glacial MIS 22a, with the terminal stadial event of Termination X, stands out as a special time. On the one hand, the highest % *N. pachyderma* and the coldest SST during a prolongated period indicate extreme cooling and incursion of subpolar waters into the latitudes of the Gulf of Cadiz. This is only possible if the subarctic front was shifted southward in the eastern North Atlantic. On the other hand, Kaiser et al. (2019) infer the subtropical gyre expanded at least as far north as 41° N, with a vigorous circulation. The % GTS data of Site U1387 agree in general with such a scenario, although

the eastern boundary of the subtropical gyre was in the vicinity of the Gulf of Cadiz only prior to and after the terminal stadial event, and a subsurface warm water body was absent during the stadial event itself. As such, the Gulf of Cadiz is once again confirmed as an important confluence region during glacial periods.

Millennial-scale climate variability is clearly recorded as stadial–interstadial SST oscillations during the transition from MIS 25 to MIS 24, whereas during the MIS 21–MIS 20 transition, only MIS 21d and MIS 21b experienced short-term cooling events. Likewise, MIS 19b was associated with a short-term cooling event.

By combining evidence from planktonic foraminifera assemblages with two types of SST reconstructions, we have identified potential biases in our reconstructions. The persistent presence of subtropical-gyre- and AzC-related species in our samples leads to overestimated PF-SSTs following the respective glacial inception and during part of the glacial periods, which becomes obvious in comparison with the $U^{k'}_{37}$-SSTs. On the other hand, the "hidden" presence of a *N. pachyderma* variant with an affinity to warmer AzC current waters, mixed in with the polar variant, probably leads to a cold bias in the PF-SST reconstructions of the extreme cold events. The temporal evolution of *N. pachyderma* and its affinities and potential implications for paleoceanographic reconstructions in the region will be explored in the future, when the Site U1387 planktonic foraminifera faunal records going back to 1500 ka have been completed.

Code and data availability. The different time series and the planktonic foraminifera faunal data with their respective LR04- and Probstack-related age models are archived in the PANGAEA world data center (https://doi.org/10.1038/s41597-023-02269-x, Felden et al., 2023) and accessible through the reference Voelker et al. (2025; https://doi.org/10.1594/PANGAEA.974451). Partial records of the *G. bulloides* oxygen isotope and $U^{k'}_{37}$ SST raw data for MIS 21-MIS 26 were already published in Bajo et al. (2020a, https://doi.org/10.1126/science.aaw1114); note that Bajo et al. (2020b, c) ages listed in PANGAEA differ from the age model(s) used in this paper: https://doi.org/10.1594/PANGAEA.914401; https://doi.org/10.1594/PANGAEA.914400. This study used the Ocean Data View software by Schlitzer (2023) available at https://odv.awi.de/.

Supplement. The supplement related to this article is available online at https://doi.org/10.5194/cp-21-919-2025-supplement.

Author contributions. AHLV initiated and designed the study and secured funding for the biogeochemical and stable isotope analyses. AM produced the planktonic foraminifera faunal data and, together with AHLV, wrote the first draft of the manuscript. ES trained AM in the application of SIMMAX and the interpretation of its results. MP produced the lipid biomarker data under the supervision of TR, who also made the final quality control of the results. HK performed the stable isotope analyses at MARUM. All authors, with the exception of MP, who has left science in the meantime, read and commented on the draft of the manuscript and approved its final version.

Competing interests. At least one of the (co-)authors is a member of the editorial board of *Climate of the Past*. The peer-review process was guided by an independent editor, and the authors also have no other competing interests to declare.

Disclaimer. Publisher's note: Copernicus Publications remains neutral with regard to jurisdictional claims made in the text, published maps, institutional affiliations, or any other geographical representation in this paper. While Copernicus Publications makes every effort to include appropriate place names, the final responsibility lies with the authors.

Acknowledgements. The samples for this study were provided by the Integrated Ocean Drilling Program (2003–2013), and we thank the Bremen Core Repository and its staff for support in sampling the sections. We thank Warley Soares, Cremilde Monteiro, and the research fellows contracted by the MOWCADYN project for help in preparing the samples in the micropaleontology and sedimentology lab at IPMA. We also thank the editor, Erin McClymont, and the two reviewers for their constructive comments that helped to improve our manuscript and Stefanie Schumacher for the efficient help in archiving our data sets in PANGAEA.

Financial support. The stable isotope and lipid biomarker analyses were made possible through the Fundação para a Ciência e a Tecnologia (FCT)-funded R&D project MOWCADYN (PTDC/MAR-PRO/3761/2012). Additional financial support from FCT was provided to the Centro de Ciências do Mar do Algarve (CCMAR) through the following projects: basic funding UIDB/04326/2020 (https://doi.org/10.54499/UIDB/04326/2020), programmatic funding UIDP/04326/2020 (https://doi.org/10.54499/UIDP/04326/2020), and the CIMAR-associated laboratory funding LA/P/0101/2020 (https://doi.org/10.54499/LA/P/0101/2020). Aline Mega was funded by FCT/CCMAR through PhD fellowship CCMAR01/UIDP/04326/2020. Antje H. L. Voelker was supported by an Investigador FCT grant (IF/01500/2014), which provided her salary during the initial phase of the study (2015–2021). The SEM work was made possible through access to the GOLD lab facilities at IPMA, funded by the EMSO-PT infrastructure project (POCI-01-0145-FEDER-022157).

Review statement. This paper was edited by Erin McClymont and reviewed by two anonymous referees.

References

Ahn, S., Khider, D., Lisiecki, L. E., and Lawrence, C. E.: A probabilistic Pliocene–Pleistocene stack of benthic $\delta^{18}O$ using a profile hidden Markov model, Dynam. Stat. Clim. Syst., 2, 1–16, https://doi.org/10.1093/climsys/dzx002, 2017.

Ambar, I., Armi, L., Bower, A., and Ferreira, T.: Some aspects of time variability of the Mediterranean Water off south Portugal, Deep-Sea Res. I, 46, 1109–1136, 1999.

Bahr, A., Kaboth, S., Hodell, D., Zeeden, C., Fiebig, J., and Friedrich, O.: Oceanic heat pulses fueling moisture transport towards continental Europe across the mid-Pleistocene transition, Quaternary Sci. Rev., 179, 48–58, https://doi.org/10.1016/j.quascirev.2017.11.009, 2018.

Bahr, A., Kaboth, S., Hodell, D. A., Zeeden, C., Fiebig, J., and Friedrich, O.: Temperature reconstruction for the Mid-Pleistocene Transition based on deep-dwelling foraminifera of IODP Site339-U1385, PANGAEA [data set], https://doi.org/10.1594/PANGAEA.882374, 2017.

Bajo, P., Drysdale, R. N., Woodhead, J. D., Hellstrom, J. C., Hodell, D., Ferretti, P., Voelker, A. H. L., Zanchetta, G., Rodrigues, T., Wolff, E., Tyler, J., Frisia, S., Spötl, C., and Fallick, A. E.: Persistent influence of obliquity on ice age terminations since the Middle Pleistocene transition, Science, 367, 1235–1239, https://doi.org/10.1126/science.aaw1114, 2020a.

Bajo, P., Drysdale, R. N., Woodhead, J. D., Hellstrom, J. C., Hodell, D. A., Ferretti, P., Voelker, A. H. L., Zanchetta, G., Rodrigues, T., Wolff, E. W., Tyler, J. J., Frisia, S., Spötl, C., and Fallick, A. E.: Oxygen isotope of planktic foraminifera Globigerina bulloides from IODP Site 339-U1387, PANGAEA [data set], https://doi.org/10.1594/PANGAEA.914401, 2020b.

Bajo, P., Drysdale, R. N., Woodhead, J. D., Hellstrom, J. C., Hodell, D. A., Ferretti, P., Voelker, A. H. L., Zanchetta, G., Rodrigues, T., Wolff, E. W., Tyler, J. J., Frisia, S., Spötl, C., and Fallick, A. E.: SST and synchronized ages from IODP Site 339-U1387, PANGAEA [data set], https://doi.org/10.1594/PANGAEA.914400, 2020c.

Baptista, L., Santos, A. M., Melo, C. S., Rebelo, A. C., Madeira, P., Cordeiro, R., Botelho, A. Z., Hipólito, A., Pombo, J., Voelker, A. H. L., and Ávila, S. P.: Untangling the origin of the newcomer *Phorcus sauciatus* (Mollusca: Gastropoda) in a remote Atlantic archipelago, Mar. Biol., 168, 1–16, https://doi.org/10.1007/s00227-020-03808-5, 2021.

Barker, S., Zhang, X., Jonkers, L., Lordsmith, S., Conn, S., and Knorr, G.: Strengthening Atlantic Inflow Across the Mid-Pleistocene Transition, Paleoceanogr. Paleoclimatol., 36, e2020PA004200, https://doi.org/10.1029/2020PA004200, 2021.

Barker, S., Knorr, G., Edwards, R. L., Parrenin, F., Putnam, A. E., Skinner, L. C., Wolff, E., and Ziegler, M.: 800,000 Years of Abrupt Climate Variability, Science, 334, 347–351, https://doi.org/10.1126/science.1203580, 2011.

Barker, S., Starr, A., van der Lubbe, J., Doughty, A., Knorr, G., Conn, S., Lordsmith, S., Owen, L., Nederbragt, A., Hemming, S., Hall, I., Levay, L., null, n., Berke, M. A., Brentegani, L., Caley, T., Cartagena-Sierra, A., Charles, C. D., Coenen, J. J., Crespin, J. G., Franzese, A. M., Gruetzner, J., Han, X., Hines, S. K. V., Jimenez Espejo, F. J., Just, J., Koutsodendris, A., Kubota, K., Lathika, N., Norris, R. D., Periera dos Santos, T., Robinson, R., Rolison, J. M., Simon, M. H., Tangunan, D., Yamane, M., and Zhang, H.: Persistent influence of precession on northern ice sheet variability since the early Pleistocene, Science, 376, 961–967, https://doi.org/10.1126/science.abm4033, 2022.

Billups, K. and Scheinwald, A.: Origin of millennial-scale climate signals in the subtropical North Atlantic, Paleoceanography, 29, 612–627, https://doi.org/10.1002/2014PA002641, 2014.

Billups, K., Hudson, C., Kunz, H., and Rew, I.: Exploring *Globorotalia truncatulinoides* coiling ratios as a proxy for subtropical gyre dynamics in the northwestern Atlantic Ocean during late Pleistocene Ice Ages, Paleoceanography, 31, 553–563, https://doi.org/10.1002/2016PA002927, 2016.

Billups, K., Vizcaíno, M., Chiarello, J., and Kaiser, E. A.: Reconstructing Western Boundary Current Stability in the North Atlantic Ocean for the Past 700 Kyr From *Globorotalia truncatulinoides* Coiling Ratios, Paleoceanogr. Paleoclimatol., 35, e2020PA003958, https://doi.org/10.1029/2020PA003958, 2020.

Carracedo, L. I., Gilcoto, M., Mercier, H., and Pérez, F. F.: Seasonal dynamics in the Azores–Gibraltar Strait region: A climatologically-based study, Prog. Oceanogr., 122, 116–130, https://doi.org/10.1016/j.pocean.2013.12.005, 2014.

Carracedo Segade, L. I., Gilcoto, M., Mercier, H., and Pérez, F. F.: Quasi-synoptic transport, budgets and water mass transformation in the Azores–Gibraltar Strait region during summer 2009, Prog. Oceanogr., 130, 47–64, https://doi.org/10.1016/j.pocean.2014.09.006, 2015.

Catunda, M. C. A., Bahr, A., Kaboth-Bahr, S., Zhang, X., Foukal, N. P., and Friedrich, O.: Subsurface Heat Channel Drove Sea Surface Warming in the High-Latitude North Atlantic During the Mid-Pleistocene Transition, Geophys. Res. Lett., 48, e2020GL091899, https://doi.org/10.1029/2020GL091899, 2021.

Chalk, T. B., Hain, M. P., Foster, G. L., Rohling, E. J., Sexton, P. F., Badger, M. P. S., Cherry, S. G., Hasenfratz, A. P., Haug, G. H., Jaccard, S. L., Martínez-García, A., Pälike, H., Pancost, R. D., and Wilson, P. A.: Causes of ice age intensification across the Mid-Pleistocene Transition, P. Natl. Acad. Sci. USA, 114, 13114–13119, https://doi.org/10.1073/pnas.1702143114, 2017.

Clark, P. U.: Ice Sheets in Transition, Science, 337, 656–658, https://doi.org/10.1126/science.1226335, 2012.

Clark, P. U., Archer, D., Pollard, D., Blum, J. D., Rial, J. A., Brovkin, V., Mix, A. C., Pisias, N. G., and Roy, M.: The middle Pleistocene transition: characteristics, mechanisms, and implications for long-term changes in atmospheric pCO_2, Quaternary Sci. Rev., 25, 3150–3184, 2006.

Clark, P. U., Shakun, J. D., Rosenthal, Y., Köhler, P., and Bartlein, P. J.: Global and regional temperature change over the past 4.5 million years, Science, 383, 884–890, https://doi.org/10.1126/science.adi1908, 2024.

Criado-Aldeanueva, F., Garcia-Lafuente, J., Vargas, J. M., Del Rio, J., Vazquez, A., Reul, A., and Sanchez, A.: Distribution and circulation of water masses in the Gulf of Cadiz from in situ observations, Deep Sea Res. II, 53, 1144–1160, https://doi.org/10.1016/j.dsr2.2006.04.012, 2006.

Curry, W. B. and Oppo, D. W.: Glacial water mass geometry and the distribution of $\delta^{13}C$ of ΣCO_2 in the western Atlantic Ocean, Paleoceanography, 20, PA1017, https://doi.org/10.1029/2004PA001021, 2005.

de Vargas, C., Renaud, S., Hilbrecht, H., and Pawlowski, J.: Pleistocene adaptive radiation in *Globorotalia truncatulinoides*: genetic, morphologic, and environmental evidence,

Paleobiology, 27, 104–125, https://doi.org/10.1666/0094-8373(2001)027<0104:PARIGT>2.0.CO;2, 2001.

Ducassou, E., Hassan, R., Gonthier, E., Duprat, J., Hanquiez, V., and Mulder, T.: Biostratigraphy of the last 50 kyr in the contourite depositional system of the Gulf of Cádiz, Mar. Geol., 395, 285–300, https://doi.org/10.1016/j.margeo.2017.09.014, 2018.

Elderfield, H., Ferretti, P., Greaves, M., Crowhurst, S., McCave, I. N., Hodell, D., and Piotrowski, A. M.: Evolution of Ocean Temperature and Ice Volume Through the Mid-Pleistocene Climate Transition, Science, 337, 704–709, https://doi.org/10.1126/science.1221294, 2012.

Expedition 339 Scientists: Site U1387, in: Proceedings IODP Exp. 339 – Mediterranean Outflow, edited by: Stow, D. A. V., Hernández-Molina, F. J., Alvarez Zarikian, C. A., and the Expedition 339 Scientists, Integrated Ocean Drilling Program Management International, Inc., Tokyo, https://doi.org/10.2204/iodp.proc.339.105.2013, 2013.

Eynaud, F., de Abreu, L., Voelker, A., Schönfeld, J., Salgueiro, E., Turon, J.-L., Penaud, A., Toucanne, S., Naughton, F., Sanchez Goni, M. F., Malaize, B., and Cacho, I.: Position of the Polar Front along the western Iberian margin during key cold episodes of the last 45 ka, Geochem. Geophys. Geosyst., 10, Q07U05, https://doi.org/10.1029/2009GC002398, 2009.

Farmer, J. R., Hönisch, B., Haynes, L. L., Kroon, D., Jung, S., Ford, H. L., Raymo, M. E., Jaume-Seguí, M., Bell, D. B., Goldstein, S. L., Pena, L. D., Yehudai, M., and Kim, J.: Deep Atlantic Ocean carbon storage and the rise of 100,000-year glacial cycles, Nat. Geosci., 12, 355–360, https://doi.org/10.1038/s41561-019-0334-6, 2019.

Felden, J., Möller, L., Schindler, U., Huber, R., Schumacher, S., Koppe, R., Diepenbroek, M., and Glöckner, F.: PANGAEA – Data Publisher for Earth & Environmental Science, Sci. Data, 10, https://doi.org/10.1038/s41597-023-02269-x, 2023.

Feldmeijer, W., Metcalfe, B., Brummer, G. J. A., and Ganssen, G. M.: Reconstructing the depth of the permanent thermocline through the morphology and geochemistry of the deep dwelling planktonic foraminifer *Globorotalia truncatulinoides*, Paleoceanography, 30, 1–22, https://doi.org/10.1002/2014PA002687, 2015.

Fiuza, A. F. G., Hamann, M., Ambar, I., del Rio, G. D., Gonzalez, N., and Cabanas, J. M.: Water masses and their circulation off western Iberia during May 1993, Deep-Sea Res. I, 45, 1127–1160, 1998.

Folkard, A. M., Davies, P. A., Fiuza, A. F. G., and Ambar, I.: Remotely sensed sea surface thermal patterns in the Gulf of Cadiz and the Strait of Gibraltar: Variability, correlations, and relationships with the surface wind field, J. Geophys. Res., 102, 5669–5683, 1997.

Frouin, R., Fiuza, A. F. G., Ambar, I., and Boyd, T. J.: Observations of a Poleward Surface Current Off the Coasts of Portugal and Spain during Winter, J. Geophys. Res., 95, 679–691, 1990.

Girone, A., De Astis, A., Sierro, F. J., Hernández-Almeida, I., Garcia, M. A., Sánchez Goñi, M. F., Maiorano, P., Marino, M., Trotta, S., and Hodell, D.: Planktonic foraminifera response to orbital and millennial-scale climate variability at the southern Iberian Margin (IODP Site U1385) during Marine Isotope Stages 20 and 19, Palaeogeogr. Palaeoclimatol. Palaeoecol., 615, 111450, https://doi.org/10.1016/j.palaeo.2023.111450, 2023.

Head, M. J. and Gibbard, P. L.: Early–Middle Pleistocene transitions: Linking terrestrial and marine realms, Quaternary Int., 389, 7–46, https://doi.org/10.1016/j.quaint.2015.09.042, 2015.

Hernández-Almeida, I., Sierro, F. J., Flores, J.-A., Cacho, I., and Filippelli, G. M.: Palaeoceanographic changes in the North Atlantic during the Mid-Pleistocene Transition (MIS 31–19) as inferred from planktonic foraminiferal and calcium carbonate records, Boreas, 42, 140-159, https://doi.org/10.1111/j.1502-3885.2012.00283.x, 2013.

Hernández-Almeida, I., Sierro, F.-J., Cacho, I., and Flores, J.-A.: Subsurface North Atlantic warming as a trigger of rapid cooling events: evidence from the early Pleistocene (MIS 31–19), Clim. Past, 11, 687–696, https://doi.org/10.5194/cp-11-687-2015, 2015.

Hernández-Molina, F. J., Sierro, F. J., Llave, E., Roque, C., Stow, D. A. V., Williams, T., Lofi, J., Van der Schee, M., Arnáiz, A., Ledesma, S., Rosales, C., Rodríguez-Tovar, F. J., Pardo-Igúzquiza, E., and Brackenridge, R. E.: Evolution of the gulf of Cadiz margin and southwest Portugal contourite depositional system: Tectonic, sedimentary and paleoceanographic implications from IODP expedition 339, Mar. Geol., 377, 7–39, https://doi.org/10.1016/j.margeo.2015.09.013, 2016a.

Hernández-Molina, F. J., Wåhlin, A., Bruno, M., Ercilla, G., Llave, E., Serra, N., Rosón, G., Puig, P., Rebesco, M., Van Rooij, D., Roque, D., González-Pola, C., Sánchez, F., Gómez, M., Preu, B., Schwenk, T., Hanebuth, T. J. J., Sánchez Leal, R. F., García-Lafuente, J., Brackenridge, R. E., Juan, C., Stow, D. A. V., and Sánchez-González, J. M.: Oceanographic processes and morphosedimentary products along the Iberian margins: A new multidisciplinary approach, Mar. Geol., 378, 127–156, https://doi.org/10.1016/j.margeo.2015.12.008, 2016b.

Hines, S. K. V., Charles, C. D., Starr, A., Goldstein, S. L., Hemming, S. R., Hall, I. R., Lathika, N., Passacantando, M., and Bolge, L.: Revisiting the mid-Pleistocene transition ocean circulation crisis, Science, 386, 681–686, https://doi.org/10.1126/science.adn4154, 2024.

Hodell, D. A. and Channell, J. E. T.: Mode transitions in Northern Hemisphere glaciation: co-evolution of millennial and orbital variability in Quaternary climate, Clim. Past, 12, 1805–1828, https://doi.org/10.5194/cp-12-1805-2016, 2016.

Hodell, D., Lourens, L., Crowhurst, S., Konijnendijk, T., Tjallingii, R., Jiménez-Espejo, F., Skinner, L., Tzedakis, P. C., Abrantes, F., Acton, G. D., Alvarez Zarikian, C. A., Bahr, A., Balestra, B., Barranco, E. L., Carrara, G., Ducassou, E., Flood, R. D., Flores, J.-A., Furota, S., Grimalt, J., Grunert, P., Hernández-Molina, J., Kim, J. K., Krissek, L. A., Kuroda, J., Li, B., Lofi, J., Margari, V., Martrat, B., Miller, M. D., Nanayama, F., Nishida, N., Richter, C., Rodrigues, T., Rodríguez-Tovar, F. J., Roque, A. C. F., Sanchez Goñi, M. F., Sierro Sánchez, F. J., Singh, A. D., Sloss, C. R., Stow, D. A. V., Takashimizu, Y., Tzanova, A., Voelker, A., Xuan, C., and Williams, T.: A reference time scale for Site U1385 (Shackleton Site) on the SW Iberian Margin, Global Planet. Change, 133, 49–64, https://doi.org/10.1016/j.gloplacha.2015.07.002, 2015.

Hodell, D. A., Crowhurst, S. J., Lourens, L., Margari, V., Nicolson, J., Rolfe, J. E., Skinner, L. C., Thomas, N. C., Tzedakis, P. C., Mleneck-Vautravers, M. J., and Wolff, E. W.: A 1.5-million-year record of orbital and millennial climate variability in the North

Atlantic, Clim. Past, 19, 607–636, https://doi.org/10.5194/cp-19-607-2023, 2023a.

Hodell, D. A., Crowhurst, S. J., Lourens, L. J., Margari, V., Nicolson, J., Rolfe, J. E., Skinner, L. C., Thomas, N. C., Tzedakis, P. C., Mleneck-Vautravers, M. J., and Wolff, E. W.: Oxgyen and carbon isotope data for the planktonic foraminifera Globigerina bulloides at IODP Site 339-U1385, PANGAEA [data set], https://doi.org/10.1594/PANGAEA.951386, 2023b.

Huber, R., Meggers, H., Baumann, K.-H., Raymo, M. E., and Henrich, R.: Shell size variation of the planktonic foraminifer *Neogloboquadrina pachyderma* sin. in the Norwegian–Greenland Sea during the last 1.3 Myrs: implications for paleoceanographic reconstructions, Palaeogeogr. Palaeoclimatol. Palaeoecol., 160, 193–212, https://doi.org/10.1016/S0031-0182(00)00066-3, 2000.

Jansen, E., Fronval, T., Rack, F., and Channell, J. E. T.: Pliocene-Pleistocene ice rafting history and cyclicity in the Nordic Seas during the last 3.5 Myr, Paleoceanography, 15, 709–721, 2000.

Johannessen, T., Jansen, E., Flatøy, A., and Ravelo, A. C.: The relationship between surface water masses, oceanographic fronts and paleoclimatic proxies in surface sediments of the Greenland, Iceland, Norwegian Seas, in: Carbon cycling in the glacial ocean: Constraints on the ocean's role in global change, edited by: Zahn, R., Pedersen, T. F., Kaminski, M. A., and Labeyrie, L., Springer Verlag, Berlin, 61–85, 1994.

Jonkers, L. and Kučera, M.: Sensitivity to species selection indicates the effect of nuisance variables on marine microfossil transfer functions, Clim. Past, 15, 881–891, https://doi.org/10.5194/cp-15-881-2019, 2019.

Kaiser, E. A., Caldwell, A., and Billups, K.: North Atlantic Upper-Ocean Hydrography During the Mid-Pleistocene Transition Evidenced by *Globorotalia truncatulinoides* Coiling Ratios, Paleoceanogr. Paleoclimatol., 34, 658–671, https://doi.org/10.1029/2018PA003502, 2019.

Kim, J., Goldstein, S. L., Pena, L. D., Jaume-Seguí, M., Knudson, K. P., Yehudai, M., and Bolge, L.: North Atlantic Deep Water during Pleistocene interglacials and glacials, Quaternary Sci. Rev., 269, 107146, https://doi.org/10.1016/j.quascirev.2021.107146, 2021.

Kroopnick, P. M.: The distribution of ^{13}C of $\sum CO_2$ in the world oceans, Deep Sea Res. A, 32, 57–84, 1985.

Kučera, M.: Planktonic Foraminifera as Tracers of Past Oceanic Environments, in: Proxies in Late Cenozoic Paleoceanography, Developments in Marine Geology, edited by: Hillaire–Marcel, C. and de Vernal, A., 1, Elsevier, 213–262, https://doi.org/10.1016/S1572-5480(07)01011-1, 2007.

Kučera, M., Weinelt, M., Kiefer, T., Pflaumann, U., Hayes, A., Weinelt, M., Chen, M.-T., Mix, A. C., Barrows, T. T., Cortijo, E., Duprat, J., Juggins, S., and Waelbroeck, C.: Reconstruction of sea-surface temperatures from assemblages of planktonic foraminifera: multi-technique approach based on geographically constrained calibration data sets and its application to glacial Atlantic and Pacific Oceans, Quaternary Sci. Rev., 24, 951–998, https://doi.org/10.1016/j.quascirev.2004.07.014, 2005.

Lisiecki, L. E. and Raymo, M.: A Pliocene-Pleistocene stack of 57 globally distributed benthic $\delta^{18}O$ records, Paleoceanography, 20, PA1003, https://doi.org/10.1029/2004PA001071, 2005.

MARGO Project Members: Constraints on the magnitude and patterns of ocean cooling at the Last Glacial Maximum, Nat. Geosci., 2, 127–132, 10.1038/ngeo411, 2009.

Marino, M., Maiorano, P., and Lirer, F.: Changes in calcareous nannofossil assemblages during the Mid-Pleistocene Revolution, Mar. Micropaleontol., 69, 70–90, 2008.

Marino, M., Maiorano, P., and Flower, B. P.: Calcareous nannofossil changes during the Mid-Pleistocene Revolution: Paleoecologic and paleoceanographic evidence from North Atlantic Site 980/981, Palaeogeography, Palaeoclimatology, Palaeoecology, 306, 58–69, https://doi.org/10.1016/j.palaeo.2011.03.028, 2011.

Martin-Garcia, G. M., Alonso-Garcia, M., Sierro, F. J., Hodell, D. A., and Flores, J. A.: Severe cooling episodes at the onset of deglaciations on the Southwestern Iberian margin from MIS 21 to 13 (IODP site U1385), Global Planet. Change, 135, 159–169, https://doi.org/10.1016/j.gloplacha.2015.11.001, 2015.

McClymont, E. L., Sosdian, S. M., Rosell-Melé, A., and Rosenthal, Y.: Pleistocene sea-surface temperature evolution: Early cooling, delayed glacial intensification, and implications for the mid-Pleistocene climate transition, Earth-Sci. Rev., 123, 173–193, https://doi.org/10.1016/j.earscirev.2013.04.006, 2013.

Morard, R., Darling, K. F., Weiner, A. K. M., Hassenrück, C., Vanni, C., Cordier, T., Henry, N., Greco, M., Vollmar, N. M., Milivojevic, T., Rahman, S. N., Siccha, M., Meilland, J., Jonkers, L., Quillévéré, F., Escarguel, G., Douady, C. J., de Garidel-Thoron, T., de Vargas, C., and Kucera, M.: The global genetic diversity of planktonic foraminifera reveals the structure of cryptic speciation in plankton, Biol. Rev., 99, 1218–1241, https://doi.org/10.1111/brv.13065, 2024.

Muglia, J. and Schmittner, A.: Carbon isotope constraints on glacial Atlantic meridional overturning: Strength vs depth, Quaternary Sci. Rev., 257, 106844, https://doi.org/10.1016/j.quascirev.2021.106844, 2021.

Müller, P. J., Kirst, G., Ruhland, G., von Storch, I., and Rosell-Melé, A.: Calibration of the alkenone paleotemperature index Uk^{37} based on core-tops from the eastern South Atlantic and the global ocean (60° N–60° S), Geochim. Cosmochim. Acta, 62, 1757–1772, https://doi.org/10.1016/S0016-7037(98)00097-0, 1998.

Naafs, B. D. A., Hefter, J., and Stein, R.: Millennial-scale ice rafting events and Hudson Strait Heinrich(-like) Events during the late Pliocene and Pleistocene: a review, Quaternary Sci. Rev., 80, 1–28, https://doi.org/10.1016/j.quascirev.2013.08.014, 2013.

Osman, M. B., Tierney, J. E., Zhu, J., Tardif, R., Hakim, G. J., King, J., and Poulsen, C. J.: Globally resolved surface temperatures since the Last Glacial Maximum, Nature, 599, 239–244, https://doi.org/10.1038/s41586-021-03984-4, 2021.

Peliz, A., Dubert, J., Santos, A. M. P., Oliveira, P. B., and Le Cann, B.: Winter upper ocean circulation in the Western Iberian Basin – Fronts, Eddies and Poleward Flows: an overview, Deep Sea Res. I, 52, 621–646, https://doi.org/10.1016/j.dsr.2004.11.005, 2005.

Peliz, A., Marchesiello, P., Santos, A. M. P., Dubert, J., Teles-Machado, A., Marta-Almeida, M., and Le Cann, B.: Surface circulation in the Gulf of Cadiz: 2. Inflow-outflow coupling and the Gulf of Cadiz slope current, J. Geophys. Res., 114, C03011, https://doi.org/10.1029/2008jc004771, 2009.

Pena, L. D. and Goldstein, S. L.: Thermohaline circulation crisis and impacts during the mid-Pleistocene transition, Science, 345, 318–322, https://doi.org/10.1126/science.1249770, 2014.

Pflaumann, U., Duprat, J., Pujol, C., and Labeyrie, L. D.: SIMMAX: A modern analog technique to deduce Atlantic sea surface temperatures from planktonic foraminifera in deep-sea sediments, Paleoceanography, 11, 15–36, 1996.

Pflaumann, U., Sarnthein, M., Chapman, M., de Abreu, L., Funnell, B., Huels, M., Kiefer, T., Maslin, M., Schulz, H., Swallow, J., van Kreveld, S., Vautravers, M., Vogelsang, E., and Weinelt, M.: Glacial North Atlantic: Sea-surface conditions reconstructed by GLAMAP 2000, Paleoceanography, 18, 1065, https://doi.org/10.1029/2002PA000774, 2003.

Railsback, L. B., Gibbard, P. L., Head, M. J., Voarintsoa, N. R. G., and Toucanne, S.: An optimized scheme of lettered marine isotope substages for the last 1.0 million years, and the climatostratigraphic nature of isotope stages and substages, Quaternary Sci. Rev., 111, 94–106, https://doi.org/10.1016/j.quascirev.2015.01.012, 2015.

Raymo, M. E., Ruddiman, W. F., Shackleton, N. J., and Oppo, D. W.: Evolution of Atlantic-Pacific δ^{13}C gradients over the last 2.5 m.y., Earth Planet. Sci. Lett., 97, 353–368, 1990.

Raymo, M. E., Oppo, D. W., Flower, B. P., Hodell, D. A., McManus, J. F., Venz, K. A., Kleiven, K. F., and McIntyre, K.: Stability of North Atlantic water masses in face of pronounced climate variability during the Pleistocene, Paleoceanography, 19, PA2008, https://doi.org/10.1029/2003PA000921, 2004.

Reagan, J. R., Boyer, T. P., García, H. E., Locarnini, R. A., Baranova, O. K., Bouchard, C., Cross, S. L., Mishonov, A. V., Paver, C. R., Seidov, D., Wang, Z., and Dukhovskoy, D.: World Ocean Atlas 2023, NCEI Accession 0270533, NOAA National Centers for Environmental Information [data set], 2024.

Relvas, P., Barton, E. D., Dubert, J., Oliveira, P. B., Peliz, A., da Silva, J. C. B., and Santos, A. M. P.: Physical oceanography of the western Iberia ecosystem: Latest views and challenges, Prog. Oceanogr., 74, 149–173, https://doi.org/10.1016/j.pocean.2007.04.021, 2007.

Rodrigues, T., Voelker, A. H. L., Grimalt, J. O., Abrantes, F., and Naughton, F.: Iberian Margin sea surface temperature during MIS 15 to 9 (580–300 ka): Glacial suborbital variability versus interglacial stability, Paleoceanography, 26, PA1204, https://doi.org/10.1029/2010PA001927, 2011.

Rodrigues, T., Alonso-García, M., Hodell, D. A., Rufino, M., Naughton, F., Grimalt, J. O., Voelker, A. H. L., and Abrantes, F.: A 1-Ma record of sea surface temperature and extreme cooling events in the North Atlantic: A perspective from the Iberian Margin, Quaternary Sci. Rev., 172, 118–130, https://doi.org/10.1016/j.quascirev.2017.07.004, 2017.

Rodrigues, T., Alonso-Garcia, M., Hodell, D. A., Rufino, M. M., Naughton, F., Grimalt, J. O., Voelker, A. H. L., and Abrantes, F. F.: A 1 Ma record of Sea Surface Temperature and extreme cooling events in the North Atlantic: A perspective from the Iberian Margin, PANGAEA [data set], https://doi.org/10.1594/PANGAEA.921577, 2020.

Rufino, M. M., Salgueiro, E., Voelker, A. A. H. L., Polito, P. S., Cermeño, P. A., and Abrantes, F.: Ocean kinetic energy and photosynthetic biomass are important drivers of planktonic foraminifera diversity in the Atlantic Ocean, Front. Mar. Sci., 9, 887346, https://doi.org/10.3389/fmars.2022.887346, 2022.

Salgueiro, E., Voelker, A., Abrantes, F., Meggers, H., Pflaumann, U., Loncaric, N., Gonzalez-Alvarez, R., Oliveira, P., Bartels-Jonsdottir, H. B., Moreno, J., and Wefer, G.: Planktonic foraminifera from modern sediments reflect upwelling patterns off Iberia: Insights from a regional transfer function, Mar. Micropaleontol., 66, 135–164, https://doi.org/10.1016/j.marmicro.2007.09.003, 2008.

Salgueiro, E., Voelker, A. H. L., de Abreu, L., Abrantes, F., Meggers, H., and Wefer, G.: Temperature and productivity changes off the western Iberian margin during the last 150 ky, Quaternary Sci. Rev., 29, 680–695, https://doi.org/10.1016/j.quascirev.2009.11.013, 2010.

Salgueiro, E., Naughton, F., Voelker, A. H. L., de Abreu, L., Alberto, A., Rossignol, L., Duprat, J., Magalhães, V. H., Vaqueiro, S., Turon, J. L., and Abrantes, F.: Past circulation along the western Iberian margin: a time slice vision from the Last Glacial to the Holocene, Quaternary Sci. Rev., 106, 316–329, https://doi.org/10.1016/j.quascirev.2014.09.001, 2014.

Sanchez, R. F. and Relvas, P.: Spring-summer climatological circulation in the upper layer in the region of Cape St. Vincent, Southwest Portugal, ICES J. Mar. Sci., 60, 1232–1250, https://doi.org/10.1016/S1054-3139(03)00137-1, 2003.

Sarnthein, M., Winn, K., Jung, S., Duplessy, J., Labeyrie, L., Erlenkeuser, H., and Ganssen, G.: Changes in east Atlantic deepwater circulation over the last 30,000 years: Eight time slices reconstructions, Paleoceanography, 9, 209–267, 1994.

Schiebel, R. and Hemleben, C.: Planktic Foraminifers in the Modern Ocean, Springer Verlag, Berlin Heidelberg, 358 pp., https://doi.org/10.1007/978-3-662-50297-6, 2017.

Schlitzer, R.: Ocean Data View, ODV Forum [code], https://odv.awi.de/ (last access: 4 May 2025), 2023.

Serrano, F. and Guerra-Merchán, A.: Sea-surface temperature for left-coiling *Neogloboquadrina* populations inhabiting the westernmost Mediterranean in the middle Pleistocene and the Pleistocene-Pliocene transition, Geobios, 45, 231–240, https://doi.org/10.1016/j.geobios.2011.04.003, 2012.

Shackleton, N. J.: The 100,000-Year Ice-Age Cycle Identified and Found to Lag Temperature, Carbon Dioxide, and Orbital Eccentricity, Science, 289, 1897–1902, 2000.

Shackleton, N. J., Hall, M. A., and Vincent, E.: Phase relationships between millennial-scale events 64,000–24,000 years ago, Paleoceanography, 15, 565–569, 2000.

Singh, A. D., Verma, K., Jaiswal, S., Alonso-Garcia, M., Li, B., and Abrantes, F.: Planktic foraminiferal responses to orbital scale oceanographic changes off the western Iberian margin over the last 900 kyr: Results from IODP site U1391, Global Planet. Change, 135, 47–56, https://doi.org/10.1016/j.gloplacha.2015.10.002, 2015.

Singh, H., Singh, A. D., Tripathi, R., Singh, P., Verma, K., Voelker, A. H. L., and Hodell, D. A.: Centennial-millennial scale ocean-climate variability in the northeastern Atlantic across the last three terminations, Global Planet. Change, 223, 104100, https://doi.org/10.1016/j.gloplacha.2023.104100, 2023.

Stein, R., Hefter, J., Gruetzner, J., Voelker, A., and Naafs, B. D. A.: Variability of surface-water characteristics and Heinrich-like Events in the Pleistocene mid-latitude North Atlantic Ocean: Biomarker and XRD records from IODP Site U1313 (MIS 16–9), Paleoceanography, 24, PA2203, https://doi.org/10.1029/2008PA001639, 2009.

Storz, D., Schulz, H., Waniek, J. J., Schulz-Bull, D. E., and Kucera, M.: Seasonal and interannual variability of the plank-

tic foraminiferal flux in the vicinity of the Azores Current, Deep Sea Res. I, 56, 107–124, 2009.

Sun, Y., McManus, J. F., Clemens, S. C., Zhang, X., Vogel, H., Hodell, D. A., Guo, F., Wang, T., Liu, X., and An, Z.: Persistent orbital influence on millennial climate variability through the Pleistocene, Nat. Geosci., 14, 812–818, https://doi.org/10.1038/s41561-021-00794-1, 2021.

Tachikawa, K., Rapuc, W., Vidal, L., Dubois-Dauphin, Q., Westerhold, T., Guihou, A., Bickert, T., Pérez-Asensio, J. N., Deschamps, P., and Skonieczny, C.: Eastern Atlantic deep-water circulation and carbon storage inferred from neodymium and carbon isotopic compositions over the past 1.1 million years, Quaternary Sci. Rev., 252, 106752, https://doi.org/10.1016/j.quascirev.2020.106752, 2021.

Tierney, J. E., Zhu, J., King, J., Malevich, S. B., Hakim, G. J., and Poulsen, C. J.: Glacial cooling and climate sensitivity revisited, Nature, 584, 569–573, https://doi.org/10.1038/s41586-020-2617-x, 2020.

Ujiié, Y., de Garidel-Thoron, T., Watanabe, S., Wiebe, P., and de Vargas, C.: Coiling dimorphism within a genetic type of the planktonic foraminifer Globorotalia truncatulinoides, Mar. Micropaleontol., 77, 145–153, https://doi.org/10.1016/j.marmicro.2010.09.001, 2010.

Vargas, J. M., Garcia-Lafuente, J., Delgado, J., and Criado, F.: Seasonal and wind-induced variability of Sea Surface Temperature patterns in the Gulf of Cadiz, J. Mar. Syst., 38, 205–219, 2003.

Ventura, C., Abrantes, F., Loureiro, I., and Voelker, A. H. L.: Data report: diatom and silicoflagellate records of marine isotope Stages 25–27 at IODP Site U1387, Faro Drift, https://doi.org/10.2204/iodp.proc.339.202.2017, 2017.

Villanueva, J., Grimalt, J. O., Cortijo, E., Vidal, L., and Labeyrie, L.: A biomarker approach to the organic matter deposited in the North Atlantic during the last climatic cycle, Geochim. Cosmochim. Acta, 61, 4633–4646, 1997.

Voelker, A. H. L. and de Abreu, L.: A Review of Abrupt Climate Change Events in the Northeastern Atlantic Ocean (Iberian Margin): Latitudinal, Longitudinal and Vertical Gradients, in: Abrupt Climate Change: Mechanisms, Patterns, and Impacts, edited by: Rashid, H., Polyak, L., and Mosley-Thompson, E., Geophysical Monograph Series, 193, AGU, Washington D.C., 15–37, https://doi.org/10.1029/2010GM001021, 2011.

Voelker, A. H. L. and Salgueiro, E.: Planktonic foraminifera assemblages in NE Atlantic and Alboran Sea surface sediments, PANGAEA [data set], https://doi.org/10.1594/PANGAEA.878069, 2017.

Voelker, A. H. L., de Abreu, L., Schönfeld, J., Erlenkeuser, H., and Abrantes, F.: Hydrographic Conditions Along the Western Iberian Margin During Marine Isotope Stage 2, Geochem. Geophys. Geosyst., 10, Q12U08, https://doi.org/10.1029/2009GC002605, 2009.

Voelker, A. H. L., Salgueiro, E., Rodrigues, T., Jimenez-Espejo, F. J., Bahr, A., Alberto, A., Loureiro, I., Padilha, M., Rebotim, A., and Röhl, U.: Mediterranean Outflow and surface water variability off southern Portugal during the early Pleistocene: A snapshot at Marine Isotope Stages 29 to 34 (1020–1135 ka), Global Planet. Change, 133, 223–237, https://doi.org/10.1016/j.gloplacha.2015.08.015, 2015a.

Voelker, A. H. L., Colman, A., Olack, G., Waniek, J. J., and Hodell, D.: Oxygen and hydrogen isotope signatures of Northeast Atlantic water masses, Deep Sea Res. II, 116, 89–106, https://doi.org/10.1016/j.dsr2.2014.11.006, 2015b.

Voelker, A. H. L., Jimenez-Espejo, F. J., Bahr, A., Rebotim, A., Cavaleiro, C., Salgueiro, E., and Röhl, U.: Data report: IODP Site U1387: the revised splice between Sections U1387B-18X-3 and U1387C-8R-3 (> 171.6 mcd), in: Proceedings of the Integrated Ocean Drilling Program, Volume 339, edited by: Stow, D. A. V., Hernández-Molina, F. J., Alvarez Zarikian, C. A., and the Expedition 339 Scientists, Integrated Ocean Drilling Program Management International, Inc., Tokyo, 1–11 pp., https://doi.org/10.2204/iodp.proc.339.204.2018, 2018.

Voelker, A. H. L., Rodrigues, T., Trotta, S., Marino, M., and Kuhnert, H.: A Southern Portuguese Margin Perspective of Marine Isotope Stage 47 – An Interglacial in the 41 kyr World, Atmosphere, 13, 1–25, https://doi.org/10.3390/atmos13091378, 2022.

Voelker, A. H. L., Mega, A., and Rodrigues, T.: Planktonic foraminifera faunal data and sea-surface temperatures for the Marine Isotope Stage (MIS) 18 to MIS 28 interval of IODP Site 339-U1387, Gulf of Cadiz [dataset bundled publication], PANGAEA [data set], https://doi.org/10.1594/PANGAEA.974451, 2025.

Westerhold, T., Marwan, N., Drury, A. J., Liebrand, D., Agnini, C., Anagnostou, E., Barnet, J. S. K., Bohaty, S. M., De Vleeschouwer, D., Florindo, F., Frederichs, T., Hodell, D. A., Holbourn, A. E., Kroon, D., Lauretano, V., Littler, K., Lourens, L. J., Lyle, M., Pälike, H., Röhl, U., Tian, J., Wilkens, R. H., Wilson, P. A., and Zachos, J. C.: An astronomically dated record of Earth's climate and its predictability over the last 66 million years, Science, 369, 1383–1387, https://doi.org/10.1126/science.aba6853, 2020.

Wharton, J. H., Renoult, M., Gebbie, G., Keigwin, L. D., Marchitto, T. M., Maslin, M. A., Oppo, D. W., and Thornalley, D. J. R.: Deeper and stronger North Atlantic Gyre during the Last Glacial Maximum, Nature, 632, 95–100, https://doi.org/10.1038/s41586-024-07655-y, 2024.

Willeit, M., Ganopolski, A., Calov, R., and Brovkin, V.: Mid-Pleistocene transition in glacial cycles explained by declining CO_2 and regolith removal, Sci. Adv., 5, eaav7337, https://doi.org/10.1126/sciadv.aav7337, 2019.

Wright, A. K. and Flower, B. P.: Surface and deep ocean circulation in the subpolar North Atlantic during the mid-Pleistocene revolution, Paleoceanography, 17, 1068, https://doi.org/10.1029/2002PA000782, 2002.